





This is to certify that the

thesis entitled

IN-SITU AFM EXAMINATION OF CALCITE NANOMORPHOLOGY  
IN THE PRESENCE OF KNOWN ANIONIC GROWTH INHIBITORS

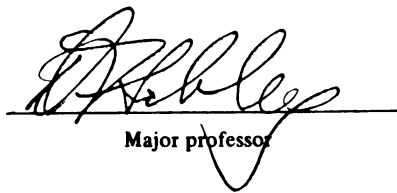
$\text{SO}_4^{2-}$  AND  $\text{PO}_4^{3-}$

presented by

Linnea J. Heraty

has been accepted towards fulfillment  
of the requirements for

Master of Science degree in Geological Sciences



Major professor

Date 5/8/98



**PLACE IN RETURN BOX**  
to remove this checkout from your record.  
**TO AVOID FINES** return on or before date due.

| DATE DUE | DATE DUE | DATE DUE |
|----------|----------|----------|
| <hr/>    | <hr/>    | <hr/>    |
| <hr/>    | <hr/>    | <hr/>    |
| <hr/>    | <hr/>    | <hr/>    |
| <hr/>    | <hr/>    | <hr/>    |
| <hr/>    | <hr/>    | <hr/>    |

**IN-SITU AFM EXAMINATION OF CALCITE  
NANOMORPHOLOGY IN THE PRESENCE OF KNOWN  
ANIONIC GROWTH INHIBITORS  $\text{SO}_4^{2-}$  AND  $\text{PO}_4^{3-}$**

By

Linnea J. Heraty

A THESIS

Submitted to  
Michigan State University  
In partial fulfillment of the requirements  
For the degree of

MASTER OF SCIENCE

Department of Geologic Sciences

1998



## **ABSTRACT**

### **IN-SITU AFM EXAMINATION OF CALCITE NANOMORPHOLOGY IN THE PRESENCE OF KNOWN ANIONIC GROWTH INHIBITORS $\text{SO}_4^{2-}$ AND $\text{PO}_4^{3-}$**

By

Linnea J. Heraty

The nanometer scale morphologic effects of two known anionic calcite growth inhibitors were observed using in situ AFM imaging. At near equilibrium, calcite saturation conditions and sulfate concentrations of 12 to 24  $\mu\text{M}$ , no effect on the morphology of calcite overgrowths was observed. Early polynuclear growth and lateral step migration morphologies were unchanged at scales of 10-1000nm in the presence of sulfate ions. This morphology is consistent with the incorporation model of growth inhibition. Contrary to sulfate results and in good agreement with previous AFM studies,  $\text{PO}_4^{3-}$  had an immediate and pronounced effect on growth morphology, producing amorphous islands and irregular steps; morphological response to a strongly adsorbed poison. A limited number of growth experiments were also performed investigating the effects of  $\text{Mg}^{2+}$ . Results were consistent with incorporation of magnesium into the calcite lattice.

**Dedicated to really little things.**

## **ACKNOWLEDGMENTS**

I would like to thank Dr. Stanley Flegler and the staff of the Center for Electron Optics at Michigan State University for their technical support in AFM operations. Many thanks to my reviewers and supporters; Dr. Neil Sturchio, Steve and Jan Armstrong, Nancy Lund, Dr. David Long and Dr. Thomas Vogel. And of course, many thanks to Dr. Duncan Sibley for coffee and tolerance.

## TABLE OF CONTENTS

|   |     |
|---|-----|
| LIST OF TABLES .....                                | vi  |
| LIST OF FIGURES .....                               | vii |
| INTRODUCTION .....                                  | 1   |
| CRYSTAL GROWTH .....                                | 6   |
| CALCIUM CARBONATE .....                             | 10  |
| INHIBITION OF CRYSTAL GROWTH .....                  | 12  |
| Incorporation Model .....                           | 12  |
| Pinning Model .....                                 | 13  |
| Cationic Inhibitors .....                           | 13  |
| Anionic Inhibitors .....                            | 16  |
| Phosphate Inhibition .....                          | 17  |
| Sulfate Inhibition .....                            | 17  |
| SCANNING FORCE MICROSCOPY .....                     | 21  |
| Principles of Operation .....                       | 22  |
| Applications .....                                  | 32  |
| MATERIALS AND METHODS .....                         | 34  |
| RESULTS AND DISCUSSION .....                        | 40  |
| General Observations .....                          | 43  |
| Malformed Faces .....                               | 49  |
| Non Doped Growth .....                              | 54  |
| Sulfate Doped Growth .....                          | 56  |
| Phosphate Doped Growth .....                        | 77  |
| Magnesium Doped Growth .....                        | 84  |
| CONCLUSIONS .....                                   | 87  |
| Nano-Morphology of Calcite in Complex Systems ..... | 87  |
| Atomic Force Microscopy .....                       | 88  |
| APPENDIX  |     |
| Force Calibration .....                             | 90  |
| LIST OF REFERENCES .....                            | 92  |

## LIST OF TABLES

|  |    |
|--|----|
| Table 1. Selected surface analytical techniques. From Hochella (1990) and Dove and Chermak (1992). .....   | 5  |
| Table 2. Average anion concentrations in surface waters. From <sup>a</sup> Stumm and Morgan (1981), <sup>b</sup> Blackburn and Dennen (1994). .....                                    | 16 |
| Table 3. Anion geometry, from Cowan et al (1990). .....  | 18 |
| Table 4. Non-doped solution general observations (C=Chihuahua Iceland Spar, R=Kola Calcite). All crystals first wetted in $\Omega=1.0$ non-doped solution unless otherwise noted ..... | 41 |
| Table 5. Doped solution general observations (C=Chihuahua Iceland Spar, R=Kola Calcite). All crystals first wetted in $\Omega=1.0$ non-doped solution unless otherwise noted .....     | 42 |

## LIST OF FIGURES

|  |    |
|--|----|
| Figure 1. Models of growth sites at step edges. (a) Block model of growth sites, shaded blocks occupy possible incorporation sites. (b) Schematic cartoons of three growth models: i mononuclear; ii polynuclear and iii spiral growth. Arrows indicate the dominant axis of material addition. .... | 9  |
| Figure 2. Profile of nonequivalent steps of a calcite monolayer. (Hillner et al, 1992). ....   | 11 |
| Figure 3. Cartoon of the underside view of an AFM cantilever and integrated pyramidal tip (after Wiesendanger, 1994). ....   | 24 |
| Figure 4. Schematic cross-section of the AFM scanning head. PSD and Laser electronics and mirrors embedded within the optical head, omitted for clarity. ....  | 25 |
| Figure 5. Ball models of tip profiles: (a) ideal, theoretical tip-sample interaction and the resulting tip path as it is scanned across the surface, shaded spheres indicate the two interacting atoms; (b) multiple tips; (c) large radius of curvature. ....                                       | 28 |
| Figure 6. False surface topography due to multiple tips. Vertical scale 50nm. ....   | 29 |
| Figure 7. Tip curvature and the resultant tip path indicated by the dashed line. Note that the shape of the tip is superimposed upon the true image. ....  | 30 |
| Figure 8. Experimental set-up for unidirectional flow of solution through the AFM fluid cell (not to scale). ....  | 38 |
| Figure 9. Step retreat with scanning at calcite supersaturation. Time elapsed from (a) to (c): 1.5 minutes. Step height at arrow = 0.36nm. ....  | 45 |

|  |    |
|--|----|
| Figure 10. Chihuahua calcite in non-doped solution (aragonite saturated) after one hour. Islands removed with subsequent scanning. Step heights on substrate 0.3 to 0.5nm, vertical relief of islands >50nm. Note the “shadows” to the right of the islands, a result of exaggerated tip force as it dropped off of the topographic high ..... | 46 |
| Figure 11. Removal of surface material due to scanning in non-doped solution at calcite saturation. Morphology obscured by scanner noise.....  | 47 |
| Figure 12. Promotion of nucleation due to scanning in non-doped solution.....  | 48 |
| Figure 13. Straight steps growing across malformed faces in non-doped solution. (A) indicates center for spiral type growth. Vertical distance between (A) and (B) = 3.2 nm. Step height at Arrow = 0.3nm. ....  | 51 |
| Figure 14. Detail of monolayer growth around irregular feature. Step height at arrow = 0.3nm.....  | 52 |
| Figure 15. Malformed features on Russian calcite in near calcite equilibrium, non-doped solution within the first 5 minutes of exposure to solution. Arrows indicate the unadulterated substrate.....  | 53 |
| Figure 16. (a) Non-doped preequilibrated crystal, vertical relief approximately 300nm. (b) Detail of the same crystal outside of the region shown in (a). ....   | 55 |
| Figure 17. Early growth features in sulfate-doped solution, (10 $\mu$ M SO <sub>4</sub> ) after 30 minutes.....  | 58 |
| Figure 18. Erosion of sulfate doped growth features due to scanning. All islands with scan region removed completely after several minutes of continuous scanning. ....  | 59 |
| Figure 19. Continued growth after exposure to sulfate; one hour in flowing, calcite saturated, non-doped solution. ....  | 60 |
| Figure 20. Polynuclear growth after 12 hours in static, non-doped solution. Note repeating feature. ....   | 61 |

|   |    |
|---|----|
| Figure 21. Distribution of nanocrystals relative to topography. Larger islands forming in depressions (lower left), while broad upper terraces are populated with small crystallites (upper right). .....       | 63 |
| Figure 22. Unaltered, initial surface before exposure to sulfate, in non-doped solution for 2 hours. ....   | 65 |
| Figure 23. Surface after 4 hours in sulfate-doped solution (10 $\mu$ M SO <sub>4</sub> ) .....  | 67 |
| Figure 24. (a)Surface after 17 hour in slowly flowing SO <sub>4</sub> -doped solution. (b) Detail of sulfate doped surface. Monolayer step height, 0.32nm. Note step morphology indicated by arrows. ....       | 68 |
| Figure 25. Initial Kola calcite surface immediately after first wetting in calcite equilibrated solution. ....  | 69 |
| Figure 26. Filling in of surface features by new growth in non-doped solution. ....   | 70 |
| Figure 27. Surface after 1 hour in flowing sulfate-doped solution (10 $\mu$ M SO <sub>4</sub> ). ....   | 71 |
| Figure 28. Tounging-island feature used to monitor growth progress. Initially imaged after 1 hour in non-doped solution. ....   | 74 |
| Figure 29. (a) Overgrowths after 1 hour in sulfate-doped solution. (b) Detail of steps imaged one minute later and outside of the region scanned in (a). Step height of pure calcite maintained at 0.38nm. .... | 75 |
| Figure 30. Overgrowths in the presence of 20 $\mu$ M SO <sub>4</sub> . (a) 30 minutes after surface flush with higher concentration solution; (b) detail of steps in adjacent region 1.5 hours later. ....      | 76 |
| Figure 31. Initial surface used for phosphate experiment: (a) within 5 minutes of first wetting in non-doped solution; (same crystal and solution after 2 hours of continuous flow. ....                        | 78 |



|   |    |
|---|----|
| Figure 32. Overgrowths in the presence of $12\mu\text{M PO}_4$ . Immediate rounding of features occurred with 5 minutes of first exposure to $\text{PO}_4$ -doped solution. ....  | 79 |
| Figure 33. Growth features after 3 hours in $\text{PO}_4$ -doped solution; (a) note unaltered substrate indicated by the arrow; (b) at lower magnification, gross-scale morphology appears unaltered. ....  | 80 |
| Figure 34. Amorphous islands covering surface in flowing $\text{PO}_4$ -doped ( $23\mu\text{M}$ ), $\text{CO}_2$ and calcite equilibrated solution after 2 hours. ....  | 81 |
| Figure 35. Distortion of mobile steps due to $\text{PO}_4$ poisoning ( $12\mu\text{M}$ ): (a) immediately after introduction of doped solution; (b) continued degradation of the surface within 2 minutes. Arrow indicates approximate scanning area of (a). .... | 83 |
| Figure 36. Mg-doped surface, somewhat obscured by noise. ....   | 85 |
| Figure 37. (a) Monolayer growth in Mg-doped ( $7\mu\text{M}$ ) solution. (b) Detail of rounded step corner. ....  | 86 |
| Figure A1. Example of Force calibration Plot generated during these experiments. $\Delta Z$ is indicated by the double-headed arrow. ....   | 91 |

## INTRODUCTION

Carbonate minerals are ubiquitous at the surface of the earth, and while simple in composition and crystalline structure, their roles in global geochemical process are quite complicated and wide reaching. Carbonates play a major role in both ground water and atmospheric chemistry. Solution chemistry of natural ground waters is controlled, in part, by carbonate-mineral hydrolysis reactions. Terrestrial and oceanic carbonate sediments also act as a major sink in the global CO<sub>2</sub> cycle.

The significance of carbonates and their role in surface water chemistries is indisputable and the kinetics of aqueous carbonate reactions have been studied extensively under laboratory conditions. Processes of nucleation, polymorph transformations, coprecipitation and bulk solution equilibria in complex solutions are all affected by the presence of foreign ions (Bischoff and Fyfe, 1968; Morse, 1983; 1990; He and Morse, 1993). However, the mechanisms of complex mineral-water interfacial reactions have not been well defined at atomic or molecular scale.

Of the numerous anhydrous carbonates, calcite is one of the most abundant rock-forming minerals and provides an excellent substrate for study of the mineral-water interface. In complex

systems (i.e. seawater), the reactivity of calcite is strongly influenced by other components in solution. The reactivity of calcite in a variety of solutions has been identified by many workers determining thermodynamic constants and rate laws (Berner and Morse, 1974; Busenberg and Plummer, 1985; Burton and Walter, 1987; Mucci et al, 1989; He and Morse, 1993; Deleuze and Brantley 1997 and many others).

Several abundant seawater electrolytes have been identified as inhibitors of calcite precipitation; including sulfate, magnesium (Bischoff and Fyfe, 1968; Mucci and Morse, 1983; Mucci et al, 1989) and orthophosphate (Berner and Morse 1974; House and Donaldson, 1985). In these studies, atomic scale physical models of growth inhibition are proposed, and for magnesium and phosphate, verified by direct observation (Gratz and Hillner, 1993; Dove and Hochella, 1993). However, the mechanism of sulfate inhibition is still explained by conjecture without the direct verification possible using Scanning Force Microscopy (SFM).

In recent years SFM has been particularly useful in the investigation of calcite surfaces and growth mechanisms (Hillner et al, 1992; Gratz et al, 1993; and Stipp et al, 1994; Liang et al, 1996) as well as imaging the micro-morphology of calcite in the presence of aqueous growth inhibitors (Dove and Hochella, 1993; Gratz and Hillner, 1993). SFM is a very effective tool in the arsenal of

technologies available for studying mineral surfaces. Scanning Force Microscopy, also referred to as Atomic Force Microscopy (actually a subset of SFM), can provide the topographic data that when coupled with other analytical methods can define and redefine (Gratz et al, 1993) mineral growth mechanisms.

Of the technologies currently available for observation of mineral surfaces at high resolutions, several are listed in Table 1. Many of these methods require ex-situ manipulation and/or destruction of the sample during preparation or analysis. Details of the *reacting* surface may be lost due to sample manipulation. Using Fluid Cell SFM, complex natural conditions can be reproduced (or approximated) and *dynamic* surfaces can be observed. SFM offers the advantage of being able to provide surface information *in situ*, without destruction or excessive modification of the surface. However, the method does have limitations; namely little chemical information can be obtained and sample-instrument interactions occur and need to be considered when interpreting images. In the study of mineral-fluid interactions, several methods must be combined in concert to overcome limitations and to verify results. As a stand alone analytical method SFM has the potential to verify or dispute proposed inhibition mechanisms due to dissolved components.

In this research, SFM technology was used to investigate the nanometer scale morphology of calcite in the presence of three

known ionic growth inhibitors: sulfate, phosphate and magnesium. A very generalized model of crystal growth includes three general reaction steps 1) transport of solutes to the interface 2) adsorption of solutes at the interface and 3) incorporation of solutes into the crystal lattice. Each step carries its own kinetic implications and in the case of calcite, these rate dynamics have been well defined. The scope of this research however, was limited to the investigation of the third, incorporation step of crystal growth. No attempt was made to quantify reaction kinetics at the mineral-water interface.

**Table 1. Selected surface analytical techniques. From Hochella (1990) and Dove and Chermak 1992).**

| Technique                              | Information                                  | Advantages  | Limitations   | Analytical Tool       |
|--|--|---|---|-----------------------|
| <b>Direct Observation</b>              |  |   |   |                       |
| Scanning Electron Microscopy (SEM)     | surface topography<br>ex-situ                | easy use, high resolution and clarity<br>limited chemical information | no height information, high vacuum<br>requires surface pretreatment | electrons             |
| Transmission Electron Microscopy (TEM) | surface topography<br>ex-situ                | molecular scale resolution  | high vacuum, destructive<br>difficult sample preparation            | electron transmission |
| Low Energy Electron Diffraction (LEED) | near-surface crystal structure<br>ex-situ    | atomic scale structure  | high vacuum<br>requires flat surface                                | electron diffraction  |
| Scanning Tunneling Microscopy (STM)    | nanometer scale topography<br>ex-situ        | molecular scale of conducting surfaces                                | cannot image insulators<br>limited chemical information             | electron tunneling    |
| Atomic Force Microscopy (AFM)          | nanometer scale topography<br>in-situ        | observe processes in real time<br>angstrom scale resolution           | minimal temperature control<br>no chemical information              | tip-sample repulsion  |
| X-ray Photoelectron Spectroscopy (XPS) | near surface chemical composition<br>ex-situ | straightforward analysis<br>depth profile to few 100 angstroms        | high vacuum   | photons/electrons     |
| Auger Electron Spectroscopy (AES)      | near surface chemical composition<br>ex-situ | straightforward analysis<br>depth profile to few 100 angstroms        | lateral resolution 100 angstrom                                     | electrons/electrons   |
| <b>Optical Microscopy</b>              |  |   |   |                       |
| Phase contrast                         | surface topography ex-situ                   | resolve monolayer steps in air  | requires careful orientation of surface                             | visible light         |
| Differential Interference Contrast     | surface topography ex-situ                   | resolve non-perpendicular edges                                       | cannot distinguish highs and lows                                   | visible light         |
| Multiple-beam Interferometry           | surface topography ex-situ                   | resolve features of a few   | requires surface pretreatment                                       | Monochromatic light   |
| <b>Indirect Observation</b>            |  |   |   |                       |
| Batch and Continuous Flow Reactors     | accurate bulk reaction rates<br><br>in-situ  | solution composition control<br>mineral-water reaction rates          | no direct mechanism information                                     | chemical reactions    |
| BET Surface Area Measurement           | total surface area<br>ex-situ                | measure of internal pore size distribution                            | bulk measurement<br>anhydrous atmosphere                            | gas                   |

## CRYSTAL GROWTH

Three models are used to describe atomic or molecular scale growth of crystals from aqueous solutions: 1) polynuclear growth; 2) mononuclear growth; and 3) spiral growth. These models all describe the addition of “building blocks” which represent single atoms or rigid molecular structural units, (i.e. the  $\text{CO}_3^{2-}$  anion) to the crystal lattice at mineral surfaces. In aqueous conditions, these building blocks or “adatoms” are supplied to the surface of the substrate crystal from solution. These adatoms may adsorb to the surface or desorb back into solution if the energy barrier to surface formation exceeds the chemical potential driving energy of the solution. Alternatively, provided the energy barrier can be overcome (including the dehydration reactions of the surface and the solutes), adatoms may become incorporated into the crystal lattice. Incorporation of a building block into the crystal lattice is most readily achieved where it is thermodynamically easiest. Steps, kinks (Figure 1a) or defects are preferred incorporation locations, providing a lower activation energy barrier to creating a new surface. Sorption on step terraces is a much less stable position and adatoms may readily desorb or they may migrate across the surface to a preferred incorporation site.

Nucleation of a new surface occurs when an adatom sorbs to the surface long enough to become a center of addition for other components. Continued accrual of building blocks progresses to form an energetically stable or critical radius if sufficient chemical supersaturation exists. The radius of this critical nucleus is a function of the interfacial energy between the crystal surface and bulk solution, and the degree of solution supersaturation. Stated more simply, how hard is it to make a new surface, and how much energy is available to drive the reaction? The free energy associated with this formation is the sum of the energy from making bonds and work in creating a new surface. As saturation increases, the activation energy barrier and critical radius size both decrease.

Once a stable nucleus has formed, growth progresses by addition of building blocks to edges and kinks around the periphery of the nucleus. Multiple nuclei may coalesce to form broad terraces. This type of growth is described by the birth-and-spread model (O'Hara and Reid, 1973); growth is initiated by surface nucleation, followed by lateral step advancement. At higher degrees of supersaturation, nucleation events can occur simultaneously with lateral step progression (polynuclear growth, Figure 1b-i). Under rare conditions (i.e. a perfect crystal substrate at low supersaturation) a single nucleus may grow laterally to complete an



entire crystal layer before another nucleation event occurs (mononuclear growth, Figure 1b-ii).

The spiral growth or BCF model, (postulated by Burton, Cabrera and Frank in 1951) has long been used to describe crystal growth for a wide range of materials, both aqueous and non-aqueous. According to the BCF model, growth is initiated at lattice defects, i.e. screw-dislocations, and is self-perpetuating (Figure 1b-iii). Continued growth is supplied by the diffusion of material across terraces to growth sites at steps: perpetual monolayer growth without nucleation. Steps at narrow terraces compete for the available adsorbed material on the adjacent terrace, and closely spaced steps should progress at a slower rate than more widely spaced steps.

The topography of the solid-liquid interface, smooth or rough will influence the dominant growth mechanism. A smooth surface provides few locations for solutes to incorporate easily into the crystal lattice. In this case, formation of a new surface by nucleation is required for growth to occur. A rough surface, with many steps will likewise provide numerous attachment sites for incoming solutes, eliminating the need for energetically expensive nucleation (Sunagawa, 1984).

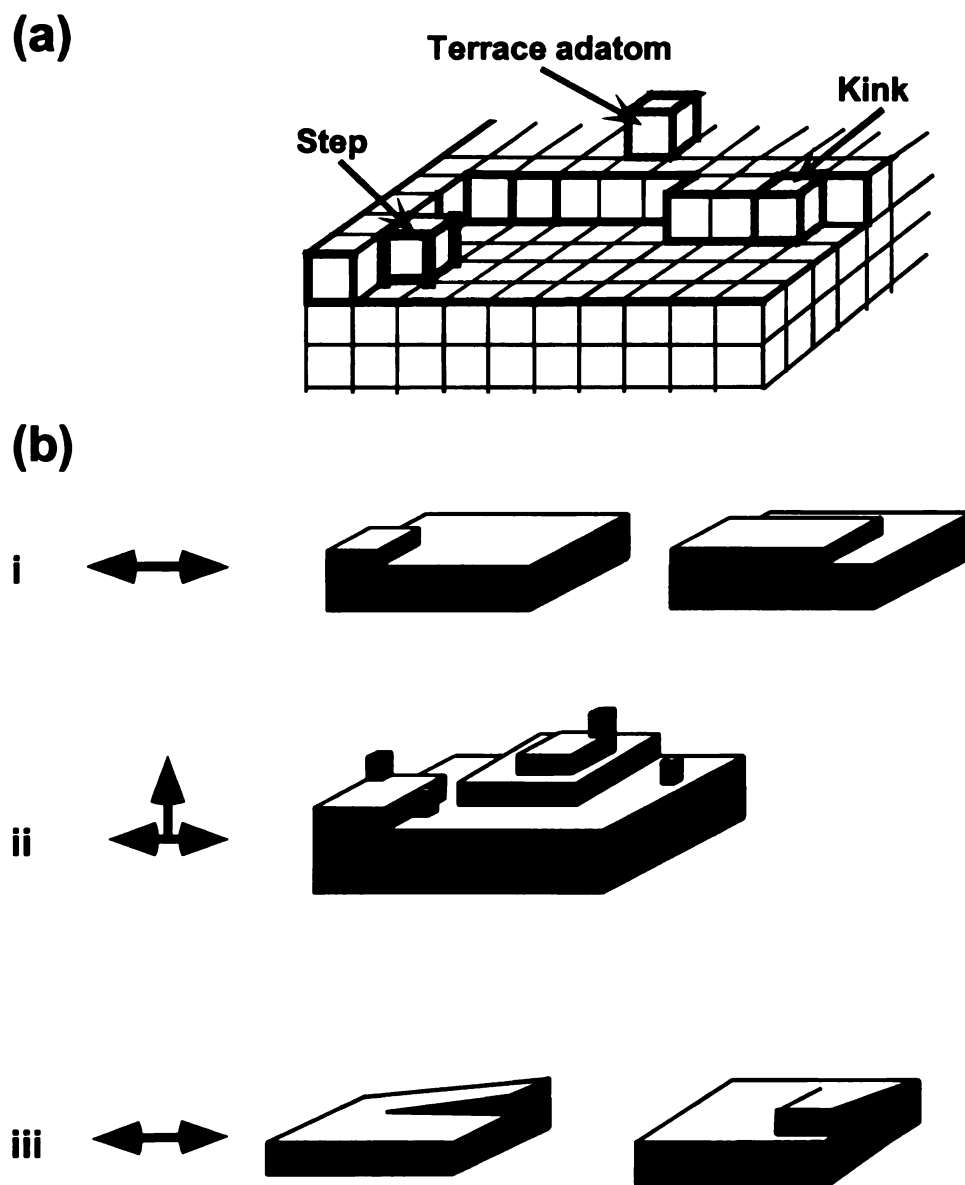


**Figure 1.** Model of growth sites at step edges. **(a)** Block model of growth sites, shaded blocks occupy possible incorporation sites. **(b)** Schematic cartoons of three growth models: **i.** mononuclear; **ii.** polynuclear and **iii.** spiral growth. Arrows indicate the dominant axis of material addition.

## CALCIUM CARBONATE

General nucleation and spiral growth models address all forms of crystal growth from vapor, solution and the melt. Crystallization of calcite under earth's surface conditions, exclusively, involves solid-solution interactions. Calcium carbonate is an ionic solid, and in many natural waters the precipitation reaction  $\text{Ca}^{2+} + \text{CO}_3^{2-} \leftrightarrow \text{CaCO}_3$  is chemically favored. The mass transfer driving force for crystal growth from aqueous solution is governed by the saturation relative to the solid phase. To describe solution conditions relative to a solid phase in non-equilibrium conditions, the saturation index ( $\Omega$ ) is used, where  $\Omega = (\{\text{Ca}^{2+}\}_{\text{act}}\{\text{CO}_3^{2-}\}_{\text{act}})/K_{\text{so}}$  which equals unity when the solid phase,  $\text{CaCO}_3$ , is in equilibrium with the solution.

There are three naturally occurring  $\text{CaCO}_3$  polymorphs; calcite, aragonite and vaterite. The thermodynamically stable species of calcium carbonate at earth surface conditions is calcite. Calcite is hexagonal in structure with the divalent calcium cations coordinated to six oxygen atoms of neighboring  $\text{CO}_3^{2-}$  anion groups, and the cations and anions layered in alternating planes. Aragonite is orthorhombic, with nine-fold cation coordination. At 25°C and 1 atm, the radius of the  $\text{Ca}^{2+}$  ion ( $\approx 1.0\text{\AA}$ ) is slightly too small for stable nine-fold coordination with the carbonate functional group. For large cations ( $>1.0\text{\AA}$ ) the six-fold coordination of calcite is not

thermodynamically stable at 25°C, therefore the aragonite structure is favored. Vaterite is similar in structure to aragonite, metastable with respect to calcite and aragonite under natural conditions (Carlson, 1983) and will not be discussed here.

The morphology of the calcite surface is governed by the planar carbonate groups that distort the structure of the bulk crystal to a rhombohedral form. At the dominant cleavage plane  $\{10\bar{1}4\}$  steps are expressed at an angle to the terrace plane (Figure 2). The difference between non-equivalent steps affects both the kinetic behavior and foreign ion incorporation within a single crystal. Impurity incorporation during crystal growth is governed in part by the structure of the substrate. In very basic terms, the steric hindrance at steps can limit the degree of foreign ion incorporation. Intrasectoral zoning, the compositional differences of different sectors on a single calcite face is dealt with in detail by Paquette and Reeder (1995 and 1990).

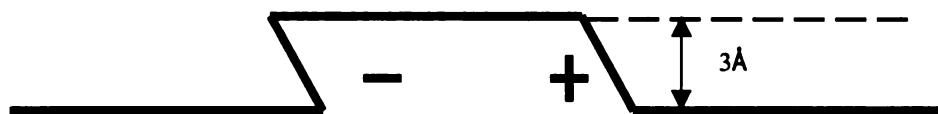


**Figure 2.** Profile of nonequivalent steps of a calcite monolayer (Hillner et al, 1992).

## **INHIBITION OF CRYSTAL GROWTH**

Foreign ions at the mineral water interface can disrupt the nucleation and growth of the bulk crystal by; adsorption at growth sites, which may distort the crystal lattice, change surface charge or complete deactivation of growth sites (Gratz and Hillner, 1993).

Two of these growth inhibition mechanisms are discussed here: 1) incorporation of foreign ions into the lattice resulting in an increase in mineral solubility and 2) pinning of growth steps by adsorption of ions at step edges. The physical behavior of foreign ions at the solid-solution interface and the mechanism of inhibition can govern the overall crystal nano-morphology of the surface. The following is a discussion of these mechanisms.

### **Incorporation Model**

According to Goldschmidt's rules of ionic substitution in crystals substitution of foreign ions in the crystal lattice is possible if the radii of two different ions differ by less than  $\cong 15\%$ . While the overall geometry of the primary crystal lattice may be maintained, incorporation of foreign ions with slightly different ionic radii can result in lattice distortions which in turn increase mineral solubility (Gratz and Hillner, 1993; Busenberg and Plummer, 1985). In this model, growth inhibition is a result of a reduction in precipitation

rates due to increased mineral solubility at the surface. The sub-angstrom distortion of the lattice is undetectable at nanometer scales and the surface morphology remains essentially unaltered from that of the pristine mineral.

### **Pinning Model**

A strongly adsorbed ion can inhibit growth by blocking or deactivating a growth site. On any given crystal, there will be a finite number of thermodynamically favorable growth sites at step edges. If any of these are occupied by strongly adsorbed foreign ions, addition of the primary mineral building blocks cannot continue at that specific site. At non-poisoned sites adjacent to the deactivated sites, growth may proceed normally. The overall observable effect, at nanometer scale, is of steps that appear to have been pinned in place, with jagged and irregular step edges.

### **Cationic Inhibitors**

In complex solutions such as seawater, many ions complicate the dynamics of crystal growth. The effects of these ions on calcite growth have been demonstrated in macro-scale kinetic studies of dissolution and precipitation. The effects of cations on calcite precipitation and dissolution have received a great deal of attention

(Berner, 1975; Mucci and Morse, 1984 and 1985; Reddy, 1986; and Burton and Walter, 1990).

It has long been known that  $\text{Mg}^{2+}$  has a marked effect on growth rates of calcite in seawater composition solutions. Bischoff and Fyfe (1968) documented the rate inhibiting effect of magnesium and Berner (1975) found that in seeded precipitation of aragonite and calcite in seawater,  $\text{Mg}^{2+}$  had a strong inhibiting effect on calcite growth rates (and no effect on aragonite growth rates). A wide body of evidence exists supporting the model that  $\text{Mg}^{2+}$  replaces  $\text{Ca}^{2+}$  in the crystal lattice producing a magnesian calcite with increased solubility. Berner (1974) predicted that the most stable Ca-Mg calcite (in seawater) contains between 2 to 7 mole percent  $\text{MgCO}_3$ , and concluded that the incorporation of magnesium produced a Mg-calcite of increased solubility, hindering calcite formation, thereby enhancing aragonite precipitation (selective polymorphism). Walter and Morse (1984) suggest that the thermodynamic equivalent point between aragonite and Mg-calcite exists up to 12 mole%  $\text{MgCO}_3$ . This magnesium-calcite selectivity was further demonstrated in Auger spectroscopic analysis of surface adsorbed layer composition of aragonite and calcite (Mucci and Morse, 1985). Their results showed that magnesium ions are adsorbed  $\approx 30$  times less than calcium on aragonite, whereas both cations are adsorbed equally on calcite.

The effects of  $\text{Mg}^{2+}$  ions have more recently been revealed by direct observation at very high resolution using SFM methods. Gratz and Hillner (1993) studied the poisoning of calcite growth by magnesium and orthophosphate as well as industrial scale inhibitors (phosphonates) using SFM. At micron scale resolution, the observable effect of magnesium was to slow step progression slightly while both rounding corners and altering macrostep formation (combination of monolayer steps to form thicker steps). In non-doped conditions, the authors observed macrostep formation only on negative direction steps (Figure 2). In the presence of magnesium macrostep formation was observed only on positive steps. Pt-C replicas of calcite surfaces imaged by transmission electron microscopy demonstrated a patchy distribution of overgrowths in magnesium doped conditions (Paquette et al, 1996). The same authors also report differential inhibition at step edges and corners in the presence of magnesium. The results of these studies suggest that the mechanism of magnesium inhibition is described by the incorporation model of crystal growth inhibition where magnesium ions are incorporated into the calcite lattice with only a slight distortion of the step edge morphology.



## Anionic Inhibitors

Of the many anions in seawater, phosphate and sulfate anions have been identified as calcite growth inhibitors (Busenberg and Plummer, 1985; Walter, 1986; Mucci et al., 1989; Didymus et al, 1993; Paquette et al, 1996). In many industrial settings, organo-phosphates are used as calcite scale inhibitors (Matty and Tomson, 1988; Gratz and Hillner, 1993). In macro scale, bulk chemical seeded growth experiments, Bischoff and Fyfe (1968) found that at varying concentrations magnesium exerted a greater inhibiting effect than sulfate. Relative to magnesium, orthophosphate is a much stronger inhibiting agent while it is much less effective than phosphonate threshold inhibitors (Gratz and Hillner, 1993). Table 2 lists the average concentrations of three important anions in natural waters and a few possible mineral sources.

**Table 2. Average anion concentrations in surface waters. From <sup>a</sup>Stumm and Morgan (1981), <sup>b</sup>Blackburn and Dennen (1994).**

| Anion                          | Seawater (M) <sup>a</sup> | Freshwater (M) <sup>a</sup> | Effect on calcite growth | Possible source <sup>b</sup>  | logK <sub>p</sub> <sup>a</sup> |
|--------------------------------|---------------------------|-----------------------------|--------------------------|---|--------------------------------|
| HCO <sub>3</sub> <sup>-</sup>  | 2.29X10 <sup>-3</sup>     | 1.00X10 <sup>-3</sup>       | promoter                 | Carbonates<br>M <sup>2+</sup> (CO <sub>3</sub> )                                    | -16.7<br>to +7.46              |
| HPO <sub>4</sub> <sup>2-</sup> | 4.99X10 <sup>-6</sup>     | 1.99X10 <sup>-4</sup>       | inhibitor                | Apatite<br>Ca <sub>4</sub> (PO <sub>4</sub> ) <sub>3</sub> (F,Cl,O<br>H)            | -114 to -118                   |
| SO <sub>4</sub> <sup>2-</sup>  | 2.82X10 <sup>-2</sup>     | 1.20X10 <sup>-4</sup>       | inhibitor                | Anhydrite(CaSO <sub>4</sub> )<br>Gypsum<br>(Ca(SO <sub>4</sub> )•2H <sub>2</sub> O) | -4.38<br>-4.60                 |

### **Phosphate Inhibition**

Several workers have suggested that adsorption of dissolved phosphate on the calcite surface deactivates potential growth sites (Bischoff and Fyfe, 1968; Berner and Morse, 1974; Walter, 1986; and Mucci et al., 1989). Scanning Force Microscopy has been used to verify this model of phosphate growth inhibition. Dove and Hochella (1993) found that when introduced during early nucleation, orthophosphate induced amorphous shaped nuclei and addition during step growth induced jagged, irregular steps. Gratz and Hillner (1993), also using SFM, imaged industrial organo-phosphate threshold poisons (whose inhibiting effects increase drastically above a threshold concentration). At high concentrations, these large compounds were visible as topographic highs at step edges. At lower concentrations, steps were jagged where growth continued between pinned regions. In the same study, naturally occurring orthophosphate did not demonstrate threshold behavior; however, the growth morphology was consistent with the pinning or poison model of crystal growth inhibition.

### **Sulfate Inhibition**

While the atomic-scale mechanism of inhibition has recently been verified for phosphate, the effects of sulfate have not yet been directly observed at the calcite-solution interface. Busenberg and

Plummer (1985) proposed that the incorporation of sulfate into the calcite lattice caused lattice distortion, which resulted in an increase in mineral solubility and reduced growth rates. Mucci et al (1989) suggested that sulfate inhibition is due to a combination of mechanisms; the adsorption of  $\text{SO}_4^{2-}$  ions by  $\text{Ca}^{2+}$  sites (poisoning) and their incorporation into the calcite lattice (increased overgrowth solubility).

Several lines of evidence suggest that sulfate ions are in fact incorporated into the calcite crystal lattice, unlike phosphate. By size and charge differences alone, it would seem apparent that sulfate could substitute for carbonate ions in the calcite lattice (Table 3).

**Table 3. Anion geometry, from Cowan et al (1990).**

| Anion               | Electrostatic radius (Å) | Geometry           | % $\text{CO}_3^{2-}$ | Charge difference |
|---------------------|--------------------------|--------------------|----------------------|-------------------|
| $\text{CO}_3^{2-}$  | 2.87                     | planar             | ---                  | 0                 |
| $\text{SeO}_3^{2-}$ | 3.18                     | Slightly nonplanar | 11                   | 0                 |
| $\text{SO}_4^{2-}$  | 3.21                     | tetrahedral        | 12                   | 0                 |
| $\text{PO}_4^{3-}$  | 3.74                     | tetrahedral        | 33                   | 1                 |

In Raman, IR Spectroscopic and chemical analysis of travertines and recent marine carbonates, Takano (1985) suggested that  $\text{SO}_4^{2-}$  replaces  $\text{CO}_3^{2-}$  in the travertine lattice, (with the substitution being easier with concurrent small cation substitution to enlarge the anion site, in agreement with Busenberg and Plummer,

1985). Crystallographic measurements of two inorganic, sulfate-containing calcite samples (up to 1.6%  $\text{SO}_4^{2-}$ ) compared to reagent Merck®, sulfate-free calcite showed a slight elongation along the c-axis (of  $\cong 0.05\text{\AA}$ ).

By comparison with other anions of similar size, evidence indicates that incorporation of sulfate is possible. Adsorption data for  $\text{SeO}_3^{2-}$  led Cowan et al. (1990) to conclude that selenite was incorporated at anion sites on calcite. Judging by size alone, sulfate should behave similarly (Table 3). This was later confirmed by x-ray standing wave studies (Cheng et al., 1997). Comparison of anion geometry also suggests the plausibility of sulfate incorporation. The large tetrahedron of  $\text{SeO}_4^{2-}$  (O-O edge length for  $\text{SeO}_4^{2-}$  is  $2.67\text{\AA}$ , while O-O edge length for  $\text{CO}_3$  is  $2.22\text{\AA}$ ) was shown to be incorporated in XAFS experiments performed on calcite (Reeder et al, 1994). The evidence that a large tetrahedron can fit into  $\text{CO}_3$  sites (with some lattice distortion) suggests that the sulfate ion may also substitute for  $\text{CO}_3$ . Furthermore, Staudt et al (1994) found that there was significant crystallographic control of both  $\text{SeO}_4^{2-}$  and  $\text{SO}_4^{2-}$  composition in calcite, indicating an interaction with the lattice structure by substitution. In their study of calcite overgrowths by Pt-C replication, Paquette et al (1996) found no observable morphological effect due to sulfate inhibition on calcite seed crystals at a scale of several microns.

SFM has the potential to identify the mechanisms of growth inhibition due to sulfate in solution by generating very high-resolution images of calcite surface morphology in doped growth solutions. Step edges and nuclei extensively altered in sulfate doped conditions would be evidence of an adsorbate blocking growth sites, as has been demonstrated in phosphate doped experiments (Dove and Hochella, 1993; Gratz and Hillner, 1993).

## SCANNING FORCE MICROSCOPY

The field of Scanning Probe Microscopy (SPM) began with the advent of the Scanning Tunneling Microscope in (STM) by Binnig, Rohrer, Gerber and Weibel in 1981. The STM retrieves sub-nanometer information of a surface by generating a tunneling electron current between a very sharp probe and a conductive solid as the probe is scanned across the surface. The tunneling current is monitored, through feed-back-loop electronics, as a function of probe position with respect to the surface (x and y directions). The physical properties of the surface atoms influence the tunneling current and the effects are translated into a three dimensional representation of the surface. Using this method, atomic scale images can be generated without damaging the surface (Wiesendanger, 1994). However, the method is limited to conductive materials.

This very elegant technique led to a Nobel Prize for its inventors in 1986, however by this time the technique had continued to develop, and its use was being expanded to be more applicable to a wider range of materials. The fathers of the STM adapted their instrument to measure ultra-small forces,  $10^{-18}\text{N}$ , on the order of interatomic interactions (Binnig et al., 1986). The STM tungsten tip was replaced by a sharp probe mounted on a soft spring

cantilever, similar to a stylus profilimeter. By replacing a rigid stylus with a soft spring cantilever, deformation of the surface being scanned was avoided, and the displacement of the spring was measured as it was scanned across the surface. In this new configuration, monitoring the interatomic forces between the sharp tip and a surface allowed nanometer scale mapping of non-conductive surfaces, giving rise to the field of Scanning Force Microscopy (Wiesendanger, 1994).

The terms Atomic Force Microscopy (AFM) and Scanning Force Microscopy (SFM) are used somewhat interchangeably to describe instrumental techniques that detect interatomic forces, with both included within the field of Scanning Probe Microscopy. SPM now encompasses a whole family of scanning methods that utilize a probe that is scanned or rastered across a sample measuring virtually any physical property of interest, including magnetism, capacitance, friction or functional group chemistry.

### **Principles of Operation**

The Atomic Force Microscope exploits the repulsive forces between the atoms of a microfine tip and a surface. This tip is mounted on a spring cantilever (Figure 3) and held in near contact with a sample surface. Then the sample is scanned or rastered in the x-y plane. As the sample and atomically sharp (theoretically) tip

come into "contact," outer shell repulsive forces cause deflections in the cantilever in the z direction. Cantilever deflection (z-axis relative to the sample) is measured by a laser, which is reflected off the back of the gold-coated cantilever, to a photo diode Position Sensitive Detector (PSD), Figure 4. The topography of the sample surface is described as a function of tip position (x-y plane) and deflection (z direction) information (Kipp et al, 1994).

At an infinite distance from the surface, the tip experiences zero deflection and the sample experiences zero force. As the tip is brought into closer "contact" with the surface, the force on the surface increases while the tip is deflected by the atom(s) of the sample. Measuring the deflection of the tip and multiplying by the spring constant of the cantilever gives the actual force experienced by the sample (Prater et al., 1995).



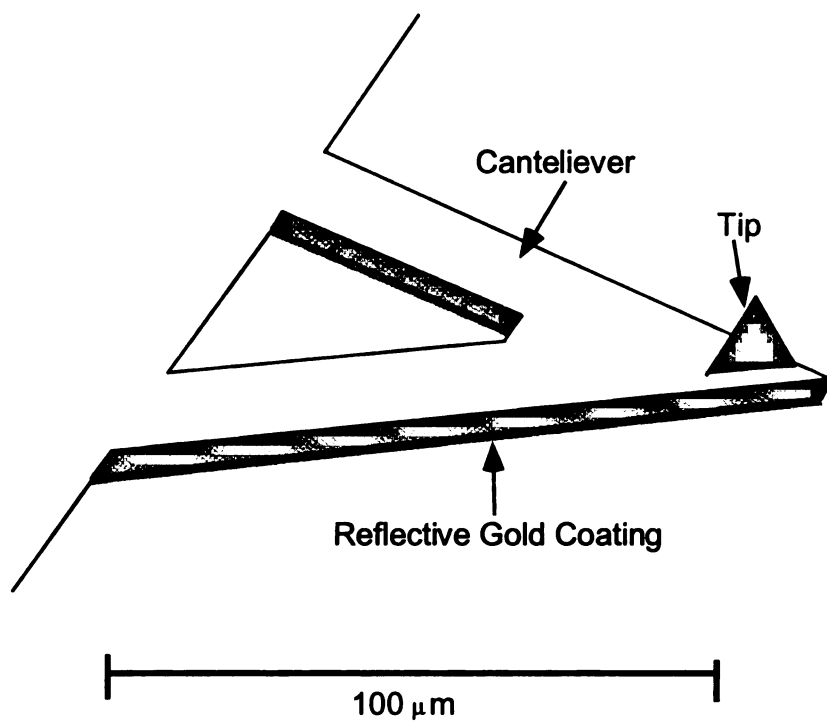


**Figure 3.** Cartoon of the underside view of an AFM cantilever and integrated pyramidal tip (after Wiesendanger, 1994).

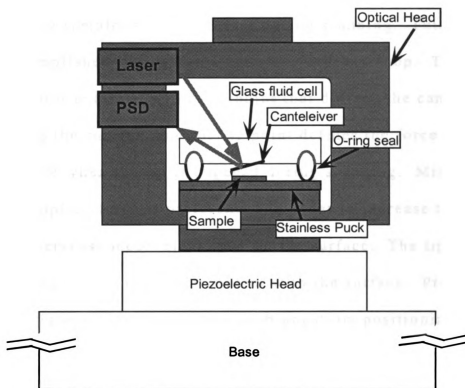


**Figure 4.** Schematic cross-section of AFM scanning head. PSD and Laser electronics and mirrors embedded within the optical head omitted for clarity.

In constant force or contact mode AFM, the force between the tip and sample is held constant during scanning. This is accomplished through an electronic feedback loop. The AFM operator enters a voltage setpoint that defines the cantilever position above the surface, and this setpoint defines the force applied to the surface when the tip is engaged during scanning. Minimization of the applied force is preferential in order to increase the sensitivity and decrease mechanical wear on the surface. The tip is engaged by moving it into very near contact with the surface. Piezoelectric translators control ultra fine, sub-angstrom positioning of the tip in three dimensions and the voltage across the piezo crystal defines tip position.

Once the tip is engaged, the surface is scanned at a moderate frequency (6 to 20 HZ). When a surface topographic-high causes the tip-sample force to increase, detected by a change in the cantilever deflection, the tip is moved away from the surface (or the surface is moved away from the tip). Similarly, if the tip-sample force is less than the setpoint the tip is moved closer to the sample and a topographic low is indicated. During scanning the position voltages are recorded with  $z$  as a function of  $x$  and  $y$ , this is then translated into a topographic map of the sample. Depending on the manufacturer of the microscope, the tip may be moved relative to the stationary sample or the sample may be moved below a stationary tip.



At very close proximity the coulombic repulsion between atom cores outweighs Van der Waals and valence shell electrostatic attractions (Wiesendanger, 1994). This repulsive force dissipates rapidly with distance, enabling the probe to precisely detect localized centers of repulsion (atoms). In this idealized scenario, only one atom of the tip would interact with one atom on the surface until the tip was moved to the next surface atom, giving atomic scale resolution (Figure 5a).

In reality, the silicon nitride ( $\text{Si}_3\text{N}_4$ ) probes commonly used often have an imperfect profile with multiple tips (Figure 5b) or broad curvature (Figure 5c). False representations of the surface due to multiple tips are identified by systematic repetition of a unique feature. Figure 6 shows what appears to be a dense field of small islands surrounding a larger island. The repeating formation and orientation of these islands is a result of a secondary tip (or tips) interaction(s) elsewhere on the surface. The step ledges seen around the larger features may be ghost steps rather than true terraces as two tips, laterally separated by approximately 50-100nm, image the same feature.

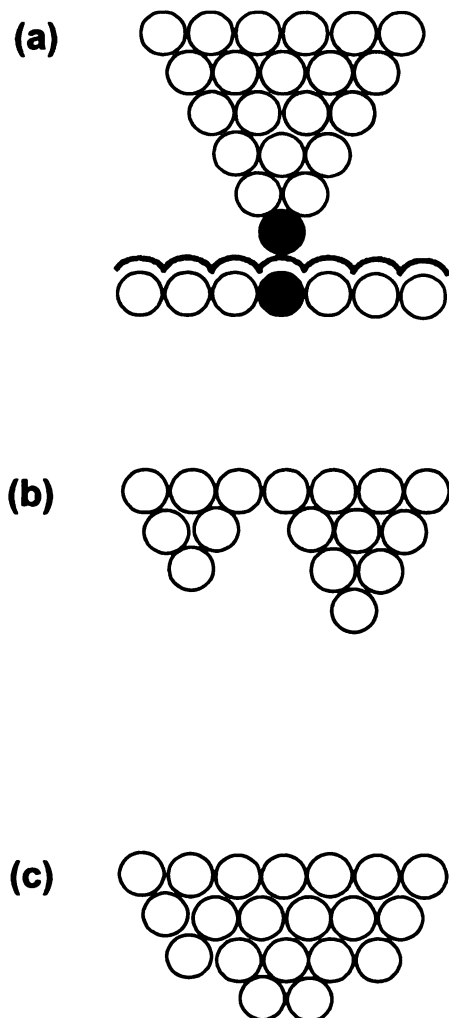


**Figure 5.** Ball models of tip profiles; (a) ideal theoretical tip-sample interaction and the resulting tip path as it is scanned across the surface, shaded spheres indicate the two interacting atoms, (b) multiple tips, (c) large radius of curvature.

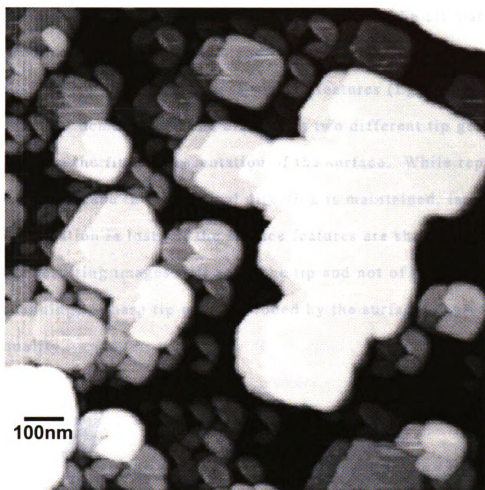


**Figure 6.** False surface topography due to multiple tips.  
Vertical scale 50nm.

Tip geometry plays an important role in the ultimate images produced during scanning. The curvature of the tip dictates the path that the tip will travel across surface features (Eggleston, 1994). Figure 7 demonstrates the effect that two different tip geometries can have on the final representation of the surface. While representation of the surface in the vertical direction is maintained, lateral information is lost. If the surface features are sharper than the tip, the resulting images will be of the tip and not of the sample. During scanning, a sharp tip may be eroded by the surface, degrading image quality.



**Figure 7.** Tip curvature and the resultant tip path indicated by the dashed line. Note how the shape of the tip is superimposed upon the true image.

Other factors, which can complicate the interpretation of images, include false engagement with fine particles on the sample (or bubbles located under the cantilever within the fluid cell) and electronic noise. Isolation from vibrations transmitted through



building foundations, or even from a ringing telephone in the next room, is necessary for very high-resolution work.

Immersing the entire system in solution can minimize most of the interference that complicates the AFM interaction. Adhesive capillary attraction can cause the tip to drag across the surface, frictional forces often cause stick-slip motion (Eggelston, 1994) and van Der Waals attraction from neighboring surface atoms reduces the precision of the tip-sample repulsion. While reducing long-range attractive forces, the fluid cell offers the added benefit of solution composition control. A fairly simple gravity feed system (Dove and Chermak, 1994) can supply a constant or changing composition solution to facilitate in situ experimentation.

The possible existence of chemical microenvironments within the cell at the sample surface and the question of solution heating by the laser or optical microscope light source are problematic when attempting to constrain near surface conditions. Flushing the cell with solution both buffers temperature changes and supplies a constant bulk-solution composition. However, while imaging during constant flow conditions is possible (Kipp et al., 1994), it is also very difficult to remain engaged with the surface and images are very noisy. Limitations of the static cell are overcome by imaging in static conditions and periodically resuming flow.

## Applications

Atomic Force Microscopy is ideally suited to study mineral surfaces *in situ*, allowing for the real-time observation of reacting surfaces. This has opened the doors to critical evaluation of crystal growth models as they pertain to real crystal systems and assisting in solving geochemical problems. In their AFM study of calcite surfaces and growth rates, Gratz et al. (1992) observed that calcite did not behave in the manner predicted by classical BCF theory. They found that steps did not interact (i.e. broad steps did not travel faster than narrow steps as is predicted in the BCF model) which indicates that material is not supplied from the terraces to growth sites at step edges. The authors therefore concluded that calcite growth occurs primarily by addition of material directly at step edges; a refinement of the BCF spiral-growth model.

Direct evidence of nucleation growth mechanisms on calcite has also been directly observed using SFM. Dove et al. (1992) observed the growth of nuclei at saturations of  $\Omega=1.0$  to 2.0 and their eventual coalescence into migrating steps after several hours. At near equilibrium conditions they suggest that growth is initiated by a short interval of surface nucleation with simultaneous dissolution and precipitation with time.

Using fluid cell AFM, molecular and atomic scale resolution is possible. However, given the physical complexity of the true tip-

sample interaction, some debate exists in the uncertainty in what the AFM probe is actually imaging; adsorbed hydration species or actual mineral constituents. Stipp et al. (1994) produced images of the calcite surface where the spacing of topographic highs agreed with unit cell dimensions, and were interpreted to be hydrated carbonate groups. By changing solution conditions, Liang et al. (1996) found that the different hydrous species did not alter surface symmetry. They concluded that the topography imaged was in fact representative of the lattice positions of the calcite constituents. Atomic scale resolution has been demonstrated on many other minerals as well. Drake et al. (1992) successfully imaged albite feldspar, rectorite, bentonite and calcite at atomic scales. Measured lateral distances of topographic features were in good agreement with predicted values for lattice spacing.

## MATERIALS AND METHODS

Two substrates were used for these experiments: Ward's Iceland Spar from Chihuahua Mexico, and calcite from the Kola Peninsula in Russia. In all experiments, blocks of calcite were ultrasonically cleaned in distilled, deionized water for 30 minutes, thoroughly rinsed and air-dried. The large blocks were then cleaved and the fragments were sorted by hand. Crystal flakes of less than one millimeter thick and approximately 3mm by 3mm with no obvious, large-scale surface defects were selected. These "fresh" dry crystal fragments were mounted on stainless steel AFM sample stubs using double-sided tape, and dusted using compressed air to remove dust particles. The crystal was then flushed with solution within the AFM fluid cell. If bubbles remained in the cell, the crystal was discarded because flushing bubbles out of the cell invariably introduced air to the surface and re-wetting consistently resulted in nucleation regardless of solution saturation.

Growth solutions were prepared by equilibrating powdered calcite or aragonite with distilled, deionized H<sub>2</sub>O (18M $\Omega$  resistance). Solutions were stirred for 2 to 3 days open to atmosphere then capped in plastic bottles for 2 to 4 weeks before being filtered with Millipore 0.45 $\mu$ m syringe filters then doped with sulfate, phosphate or magnesium stock solution. Doped solutions were used within 1 to

2 days. A small number of experiments were performed using solutions prepared by bubbling wetted CO<sub>2</sub> through calcite or aragonite suspensions in distilled, deionized water for 12 to 24 hours, then filtered. Saturation relative to calcite increased as these solutions degassed.

The ambient temperature in the laboratories where solutions were prepared and in the AFM lab, varied on a daily basis. Solution temperatures varied over ten degrees, from 20°C to 30°C. Therefore, some rather large assumptions were made regarding solution saturation. For solutions prepared by equilibration with a solid phase at atmospheric P<sub>CO2</sub>, it was assumed that the quotient of the solid solubility product (K<sub>calcite</sub> or K<sub>aragonite</sub>) and the solubility product of calcite (K<sub>calcite</sub>) was a good approximation of saturation conditions. Values for the pH of these solutions measured immediately prior to introduction into the fluid cell, fell within a range agreeable with this assumption (pH≈8).

For solutions equilibrated with elevated P<sub>CO2</sub>, saturation was approximated as a function of calcium concentrations calculated for the pH and P<sub>CO2</sub> of the solution before filtration. Carbonate values were calculated for atmospheric P<sub>CO2</sub> and the pH of the fluid cell effluent. These solutions were unstable and therefore any saturation ascribed to these solutions is approximate at best. For the range of pH values of the CO<sub>2</sub>-H<sub>2</sub>O-aragonite solutions (pH 5.7 to 6.1) and the

average pH of filtered and degassed solutions at the time of imaging (pH 7.8) calculated values of  $\Omega$  vary from 1.6 to 10.5. Depending on the degree that the solutions degassed, before use or within the fluid cell, saturations may have exceeded 20 or more. For simplicity, given that relatively few of these experiments were performed, these solutions are described as supersaturated with a  $\Omega > 1.5$ .

Dopants were prepared by dissolving reagent grade salts ( $\text{Na}_2\text{SO}_4$ ,  $\text{MgCl}_2 \cdot 6\text{H}_2\text{O}$  or  $\text{Na}_3\text{PO}_4 \cdot 12\text{H}_2\text{O}$ ) in distilled, deionized  $\text{H}_2\text{O}$  to make stock solutions of  $656\mu\text{M PO}_4^{2-}$ ,  $1035\mu\text{M SO}_4^{2-}$  and  $731\mu\text{M Mg}^{2+}$ . These stock solutions were stored in plastic bottles and diluted (100X) into filtered growth solutions directly before imaging.

With the fluid cell assembled and the sample mounted in the fluid cell, solutions were introduced to the sample using a burette equipped with 1/8" Teflon tubing and a variable screw clamp to control flow rates (Figure 8). Clamping the line below the fluid cell reduced air bubble formation within the cell by creating a slight head pressure above the cell. The experimental set-up for this study was adapted from Dove and Chermak (1994) and Kipp et al (1994).

A NanoScope III AFM equipped with a  $\approx 1.0\text{mL}$  glass fluid cell and a Digital Instruments "D" scanner (an Inver cylinder with a single tube piezo for three-dimensional control) was used for all experiments. Image processing was performed within the NanoScope AFM control software to mathematically smooth the data to a plane

by subtracting a best-fit plane derived from the data. Image files were transferred to disk and minor contrast adjustments were performed using NIH Image 1.60 freeware (Rasband, 1997). Canvas 3.5.1 (Deneba software) was used for final annotation and printing.

Growth experiments began by rinsing the sample crystal with solution just long enough to confirm the absence of bubbles. Then, with flow stopped, the  $\text{Si}_3\text{N}_4$  tip was engaged to image the initial surface (time = zero). The tip was then disengaged and solution flow resumed at  $<2.0\text{mL/min}$ . At flow rates of less than  $1.5\text{mL/min}$  it was possible to continuously image the surface (faster flow rates degraded images or completely disengaged the tip from the surface). When changing solutions during an experiment the new solution was rapidly flushed through the cell with the tip disengaged. To displace the  $1.3\text{mL}$  volume of the fluid cell and connecting tubing, first small aliquots ( $4 \times 2\text{ mL}$ ), then in larger volumes, were added through the burette, maintaining a constant flow to ensure that no air entered the line.

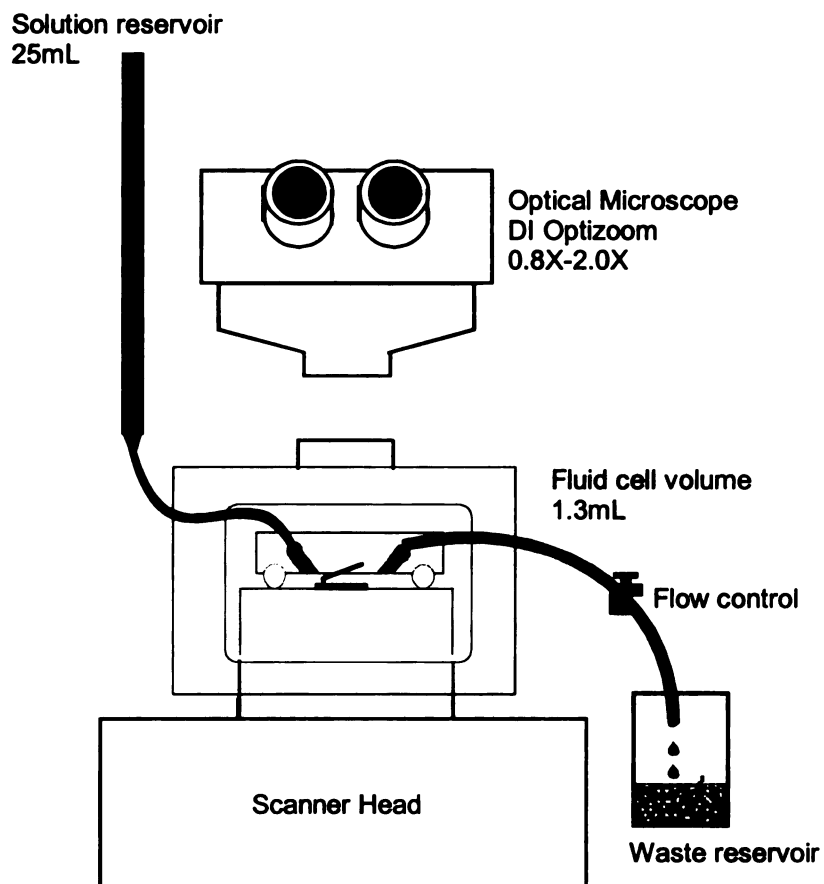


**Figure 8.** Experimental set-up for unidirectional flow of solution through the AFM fluid cell (not to scale).



For very long duration experiments the tip was re-engaged periodically as the experiment progressed, “landing” within 200-300nm of the original location scanned at time = zero. Alternatively, scanning was continuous on a small area (<200nm) adjacent to the time = zero area, moving the tip to the features of interest just long enough to capture an image (Kipp et al., 1994 and Liang et al., 1996).

In all AFM sessions, scanning conditions were optimized on an area of the crystal near the feature of interest, and the forces exerted on the surface by the tip were minimized to reduce alteration of the surface. Forces ranging from 5-20 nN were employed for these experiments. Force calibrations were performed when scanning conditions were optimized for each new sample. Total force was calculated using a spring constant ( $k$ ) of 0.06 (Digital Instruments, 1995). See Appendix for a description of force calculation.

Attempts were made to minimize thermal inputs into the fluid cell. The optical microscope light source was turned off when not required, however it could only be assumed that solution flow was sufficient enough to carry away excess heat generated within the sample cell by the laser. Temperatures of the effluent solutions ranged from 23°C to 30°C (depending on the season), and a temperature of 25°C was assumed for all experiments.

## RESULTS AND DISCUSSION

Four sets of near equilibrium growth experiments were performed: 1) non-doped; 2) phosphate-doped; 3) sulfate-doped and 4) magnesium-doped (see Table 4 and Table 5). The focus of this study was to investigate sulfate, a known anionic inhibitor, and to compare its effects to those of phosphate on the nanomorphology of calcite. Non-doped and Mg-doped experiments were performed primarily to demonstrate comparability to other AFM studies and to demonstrate inhibition models. To minimize intra-experiment “misdiagnosis” (i.e. it is very easy to find an amorphous feature with AFM), results were verified by imaging an unaltered feature on the surface. This was accomplished by imaging the surface before doped solution was added and by dissolving or re-growing with clean solution after doping the surface.

**Table 4. Non-doped solution general observations (C= Chihuahua Iceland Spar, R= Kola Calcite) All crystals first wetted in  $\Omega=1.0$  non-doped solution, unless otherwise noted.**

| <b>Solution</b>            | <b>Substrate</b>  | <b>Dominant Growth Mechanism</b> | <b>Morphology/Remarks</b>                          | <b>Figure #</b> |
|----------------------------|-------------------|----------------------------------|--|-----------------|
| <b>calcite saturated</b>   | C fresh crystal   | polynuclear                      | angular  | 32              |
|                            | C fresh crystal   | polynuclear                      | regular  | 31              |
|                            | C prewetted       |                                  | removal with scanning                              | 11              |
|                            | R fresh crystal   |                                  | very angular features, retreat with scanning       | 9               |
|                            | R preequilibrated |                                  | one week in solution, slightly more stable surface |                 |
|                            | R fresh crystal   | lateral step progression         | regular  |                 |
|                            | C fresh crystal,  | lateral + spiral growth?         | regular, malformed faces                           | 13, 14          |
|                            | R fresh crystal   | lateral step progression         | regular  |                 |
| <b>aragonite saturated</b> | C prewetted       |                                  | scanning away features                             | 9               |
|                            | C fresh crystal   | polynuclear + lateral step       | regular  | 10              |
|                            | C prewetted       | polynuclear + lateral step       | effluent pH=7.86                                   |                 |
|                            | C prewetted       | nucleation                       | possible multiple tip                              |                 |
|                            | C prewetted       |                                  |  |                 |
|                            | C prewetted       | polynuclear                      | higher density of nuclei on upper terraces         |                 |
| <b>super-saturated</b>     | C preequilibrated | polynuclear                      | regular  | 16              |
|                            | C preequilibrated | polynuclear                      | promotion of nucleation due to tip                 | 12              |

**Table 5. Doped solution general observations (C= Chihuahua Iceland Spar, R= Kola Calcite). All crystals first wetted in  $\Omega=1.0$  non-doped solution, unless otherwise noted.**

| Solution                   | Dope $\mu\text{M}$ | Substrate                              | Dominant Growth Mechanism   | Remarks/Morphology  | Figure # |
|----------------------------|--------------------|--|-----------------------------|---|----------|
| <b>Sulfate Doped</b>       |                    |  |                             |   |          |
| <b>calcite saturated</b>   | 10                 | C fresh crystal                        | polynuclear                 | regular   | 23       |
|                            | 10                 | R fresh crystal                        | lateral step progression    | broad regular terraces, tip effects                           | 27       |
|                            | 10                 | R fresh crystal                        | lateral step progression    | malformed faces   |          |
|                            | 10                 | R fresh crystal                        | lateral step progression    | tonguing island, regular steps                                | 28       |
|                            | 20                 | R fresh crystal                        | lateral step progression    | regular, some amorphism?                                      | 30       |
| <b>aragonite saturated</b> | 10                 | C fresh crystal                        | polynuclear                 | amorphous nuclei on clean background, removed by flushing     | 17-20    |
|                            | 10                 | R wetted in $\text{SO}_4$ , $\Omega=1$ | polynuclear                 | regular   | 24       |
|                            | 10                 | R                                      |                             | some nucleation with straight steps                           |          |
| <b>super-saturated</b>     | 2                  | C                                      |                             |   |          |
|                            | 10                 | C                                      |                             | surface removal scanned in regions, re-wetted during scanning |          |
|                            | 14                 | C 24 hours at $P_{\text{CO}_2}=1$      |                             | coalescing nuclei   |          |
| <b>Phosphate Doped</b>     |                    |  |                             |   |          |
| <b>calcite saturated</b>   | 6                  | R                                      |                             | poor engagement   |          |
|                            | 12                 | C                                      | polynuclear                 | amorphous nuclei, straight steps                              | 32, 33   |
| <b>aragonite saturated</b> | 23                 | C                                      |                             | thick step edges  |          |
| <b>super-saturated</b>     | 23                 | C fresh crystal                        | polynuclear                 | amorphous nuclei  | 34       |
|                            | 12                 | C                                      | lateral step progression    | irregular steps, malformed substrate not removed by scanning  | 35       |
|                            | 14                 | C capped vial 2 weeks                  |                             | bulbous steps   |          |
| <b>Magnesium Doped</b>     |                    |  |                             |   |          |
| <b>calcite saturated</b>   | 7                  | C                                      | polynuclear                 | tip artifact, regular + blurred nuclei                        |          |
|                            | 7                  | R fresh crystal                        | lateral step progression    | straight steps rounded corners                                | 37       |
| <b>aragonite saturated</b> | 7                  | R                                      | nucleation with step growth | poor engagement, repeating tip artifact                       |          |

## **General Observations**

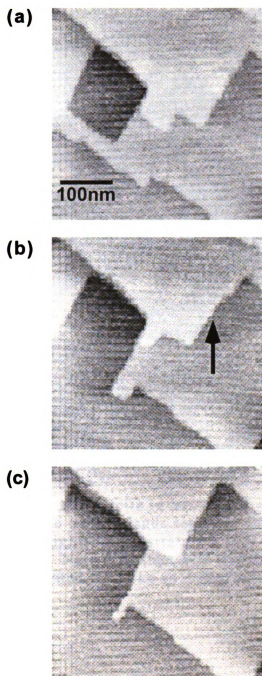
The majority of experiments were performed at near calcite equilibrium conditions using calcite or aragonite equilibrated solutions at atmospheric  $P_{CO_2}$  (relative to calcite calculated saturation indices of  $\Omega = 1.0$  to  $1.5$ , respectively). The calcite surface proved to be very reactive and sensitive to probe disturbance under these conditions. Large features, 50-100 nm wide, were easily eroded by continuous scanning, while adjacent areas of the surface continued growing, evidenced by increased size and density of nucleation and or filling in of surface features.

Simultaneous precipitation and dissolution (Dove and Hochella, 1993) is demonstrated in an experiment with aragonite equilibrated solutions. Figure 9 shows, in sequence, the rapid step retreat with three consecutive slow scans (total time elapsed; 1.5 minutes). Adjacent areas (within  $1\mu m$ ) exhibited 25-50nm islands (Figure 10) which were quickly removed by scanning, suggesting that simultaneous dissolution and re-precipitation was occurring at the surface.

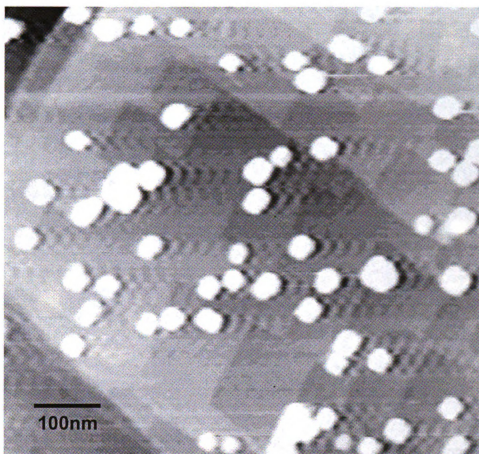
Further examples of the reactivity of the calcite surface demonstrates the need to consider the AFM tip as an active participant in surface reactions. In near equilibrium experiments, significant erosion of surface features during scanning was observed. This probe assisted dissolution is most clearly demonstrated by

Figure 11, where several hundred nanometers of new growth was removed with scanning at a supersaturation of 1.5 with respect to calcite. On the other hand, at a higher supersaturation (solution degassing from  $P_{CO_2} \approx 1 \text{ atm}$ ) the surface not only became more stable and resistant to scanning, but the tip catalyzed nucleation. Figure 12 shows a broad view of this tip assisted nucleation (image region rotated to show the region scanned continuously for 5 minutes). The force exerted on these two different samples was comparable at approximately 5nN.

The majority of experiments started by imaging the surface in non-doped, calcite equilibrated solution in order to characterize the initial surface, followed by addition of the experimental solution. The two calcite substrates studied exhibited very different initial growth mechanisms. Early growth on the Chihuahua Iceland Spar was predominantly by nucleation and island formation. The higher quality (Sturchio 1997, personal communication) Kola calcite exhibited growth by lateral step progression. The quality of the two different calcite samples had a strong control of growth mechanism.



**Figure 9.** Step retreat with scanning at calcite supersaturation. Time elapsed from (a) to (c): 1.5 minutes. Step height at arrow = 0.36nm.



**Figure 10.** Chihuahua calcite in non-doped solution (aragrite saturated) after one hour. Islands removed with subsequent scanning. Step heights on substrate 0.3 to 0.5nm, vertical relief of islands >50nm. Note the "shadows" to the right of the islands, a result of exaggerated tip force as it dropped off of the topographic high.



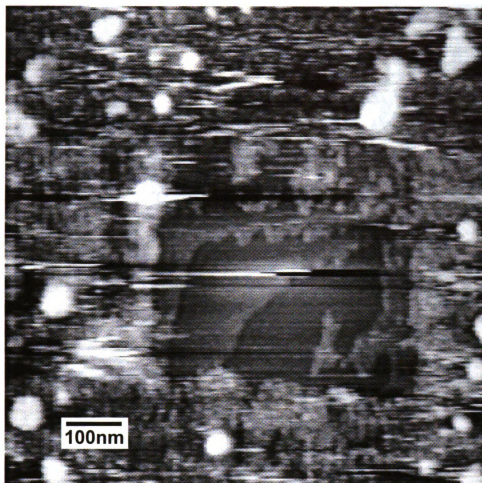


**Figure 11.** Removal of surface material due to scanning in non-doped solution at calcite saturation. Morphology obscured by scanner noise.

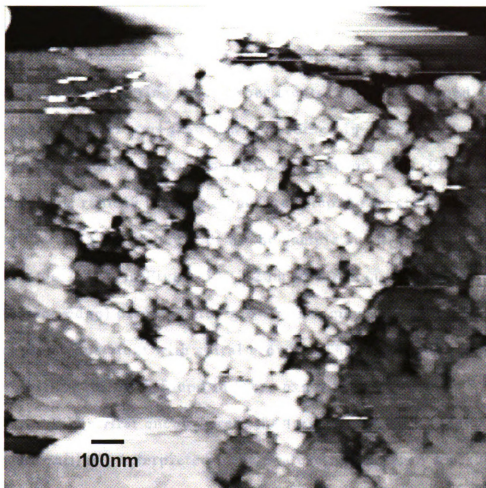


**Figure 12.** Promotion of nucleation due to scanning in super-saturated, non-doped solution.

## **Malformed Faces**

Figures 13, 14 and 15 show malformed features encountered several times during these experiments, all in non-doped solutions. Perfect lateral step growth was observed in non-doped calcite saturated solution with no initial nucleation stage (Figure 13). Straight, rapidly moving monolayer steps grew around and piled up at the irregular boundaries of the sample substrate. The lower terrace shown in Figure 13 (3.2nm lower than the irregular upper-terrace edge) displays step growth that may be centered on a screw center, consistent with spiral growth. This is the only evidence of spiral type growth found in these experiments.

When first encountered, the large irregularly shaped islands were initially interpreted to be coalescing nuclei or a result of contaminated solution and unfortunately, this sample was discarded. However, while extra care was taken to decontaminate samples and solution apparatus, these same features were encountered again on other substrates and at other saturations. Figure 14 shows a monolayer growing around an "irregularity". Amorphous features were also found superimposed over the features of Kola calcite (Figure 15). Note that all of these examples were freshly prepared "dry" cleavage fragments. The amorphous features were present on the surface of the fresh crystal at the first imaging of the surface in non-doped solution, and were resistant to removal by scanning.

Without performing additional chemical or structural analysis of these overgrowths, it is interpreted that they are a remnant of sample preparation. Large blocks of calcite were sonicated in distilled water multiple times and oven dried. No effort was made to deselect the outside surfaces of the calcite blocks before cleaving off fragments. The malformed faces likely formed on the block surfaces during the drying stage as the water film evaporated, perhaps initiating birth and spread type growth (Bosbach et al, 1996). Gratz et al (1992) observed that growth over defective regions produced atomically smooth regions of defective material in a very complex manner. Further investigation of these surfaces using AFM coupled with other surface analysis technologies would be interesting and relevant to the study of diagenetic environments.

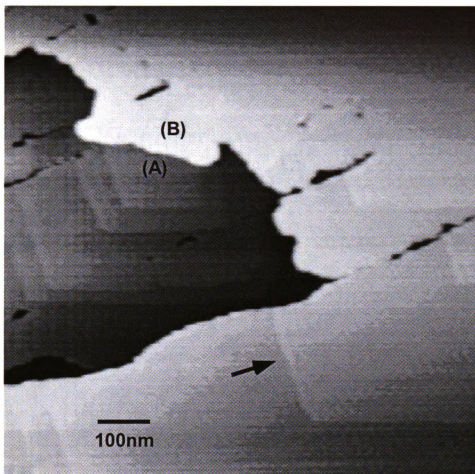


**Figure 13.** Straight steps growing across malformed faces in non-doped solution. (A) indicates center for spiral type growth. Vertical distance between (A) and (B) = 3.2 nm. Step height at arrow=0.3nm.

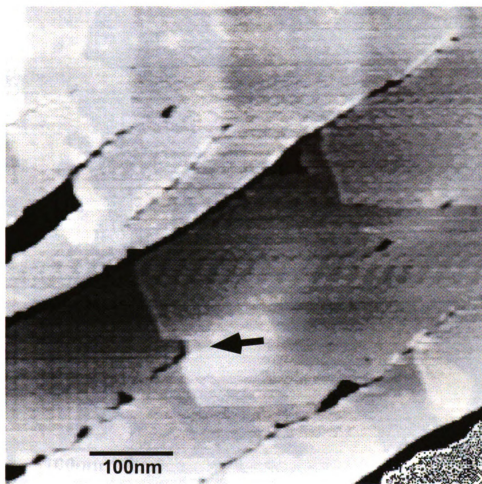


**Figure 14.** Detail of monolayer growth around malformed features. Step height at arrow= 0.3nm.

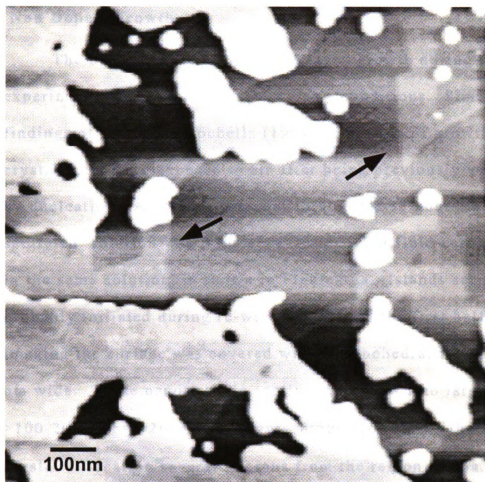


**Figure 15.** Malformed features on Russian calcite, in near calcite equilibrium, non-doped solution within first 5 minutes of exposure to solution. Arrows indicate unadulterated substrate.

## **Non Doped Growth**

The best example of nucleation type growth during these experiments was found under re-wetting conditions. Similar to the findings of Dove and Hochella (1993), initiation of growth on crystals that were exposed to air after being previously wetted was by nucleation. A crystal, pre-equilibrated for 33 hours in aragonite saturated solution was transferred to the AFM fluid cell and imaged in the same solution, is shown in Figure 16a. Islands seen here were probably initiated during re-wetting. Within the first half-hour of imaging the surface was covered with rhombohedral islands <30-40 nm wide. These nanocrystals continued to grow into larger islands >100-200nm by  $\approx$ 200nm in height. Figure 16b shows the same crystal at location several microns from the region in 16a.



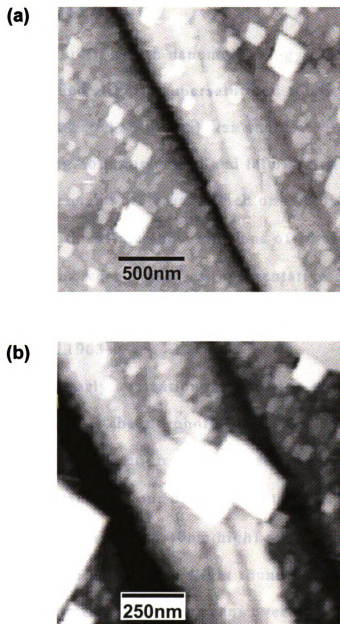


**Figure 16.** (a) Non-doped preequilibrated crystal, vertical relief approximately 300nm; (b) Detail of the same crystal outside of the region shown in (a).

## **Sulfate Doped Growth**

The overall growth nanomorphology of calcite at near equilibrium and slightly supersaturated conditions (calcite and aragonite saturated solutions) was unaffected by the presence of sulfate during both nucleation and lateral step growth. Sulfate-doped growth experiments were performed on two different calcite substrates with sulfate concentrations of 10 and 20  $\mu\text{M}$ . The sulfate concentrations were chosen as representative of the lower range of sulfate concentrations in natural surface waters (Brewer, 1975 and Livingstone, 1963).

During early nucleation the addition of sulfate did not significantly alter the morphology of new growth features. Figure 17 shows islands initiated in aragonite saturated, non-doped solution during the first half-hour of exposure to sulfate (10  $\mu\text{M}$ ). These islands ( $\leq 50\text{nm}$  wide and 40nm high) were removed with continued scanning. Figure 18 shows slight rounding of the nuclei that increased with the number of scans over the imaged area.

Flushing the surface with non-doped solution, at the same saturation, and allowing growth to continue for  $\approx 1$  hour (under constant flow of 2.0 ml/min) did not improve the apparent morphology of the surface as shown in Figure 19. Therefore, the amorphous morphology is attributed to degradation of the tip to a large radius of curvature, rather than any sulfate effect. Leaving the

same crystal in static non-doped solution for 12 hours continued polynuclear growth with nucleation and growth occurring atop previously formed islands (Figure 20). Close inspection of the features in Figure 20 suggests the presence of a tip artifact. The repeating asymmetry, most evident on the islands at the top of the figure, lends further indication of a bad tip.

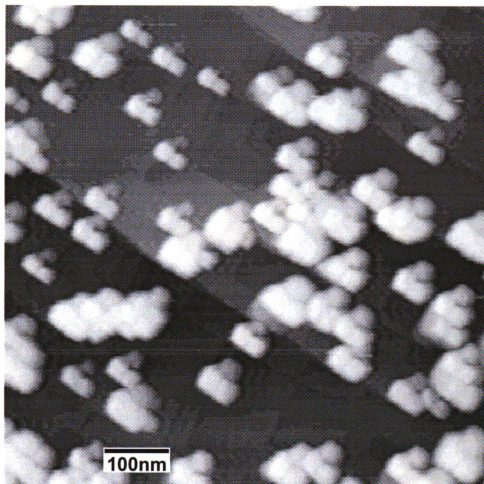


**Figure 17.** Early growth features in sulfate doped solution, ( $10\mu\text{M SO}_4$ ) after 30 minutes.

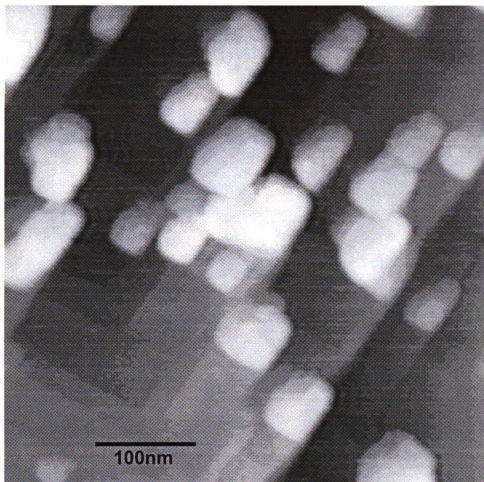


**Figure 18.** Erosion of sulfate doped growth features due to scanning. All islands within scan region removed completely after several minutes.

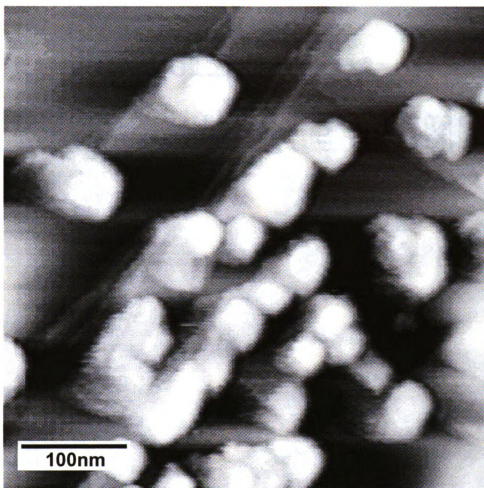


**Figure 19.** Continued growth after exposure to sulfate; one hour in flowing, calcite saturated, non-doped solution.

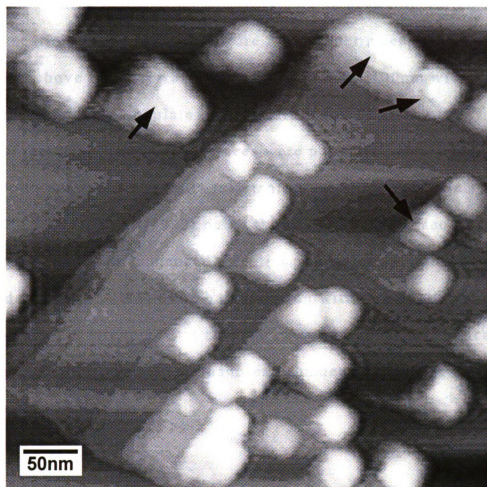


**Figure 20.** Polynuclear growth after 12 hours in static, non-doped solution. Note repeating feature.

Size distribution and resistance to scanning varied with location on the surface (Figure 21). Upper macro terraces (10 to 15 nm above lower terraces) had many broad, >100nm wide steps that were sparsely populated with small nanocrystals (upper right of figure 21). The lower terraces were populated with islands that were both numerous and more resistant to scanning (lower left of figure 21). Gratz et al (1992) noted the filling in of surface pits during step growth, citing “enhanced effective saturation in a concave depression”. While the bulk solution within the cell was replaced every 1-2 minutes, it is nevertheless apparent that chemical microenvironments (or “nano-environments”) exist at the solid-solution interface.



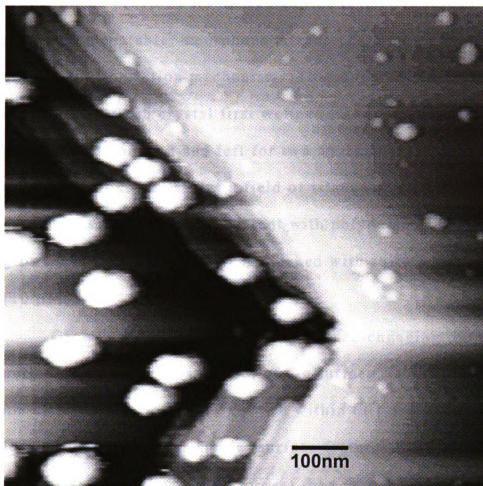


**Figure 21.** Distribution of nanocrystals relative to topography. Larger islands forming in depressions (lower left), while broad upper terraces are populated with small crystallites (upper right).

In the previous set of figures, the true morphology is somewhat debatable, amorphous islands could be a product of tip shape or of inhibition mechanism. Therefore, the experiment was repeated. A fresh crystal first wetted in non-doped calcite equilibrated solution and left for two hours in slowly flowing solution. Figure 22 shows a field of islands of varying lateral dimensions, 30-250nm, consistent with polynuclear birth-and-spread growth. This surface was then flushed with sulfate doped solution (10  $\mu$ M).

Growth progress was monitored by re-engaging the tip periodically to take a snapshot of the surface, landing within 200-300 nm of the initial location. Growth within this pre-scanned area was less rhomboid and less stable (surface features were easily removed even at very small scanning forces) than in areas more than 1-2  $\mu$ m away. In previously unscanned regions, nuclei were rhomboid and more resistant to scanning.

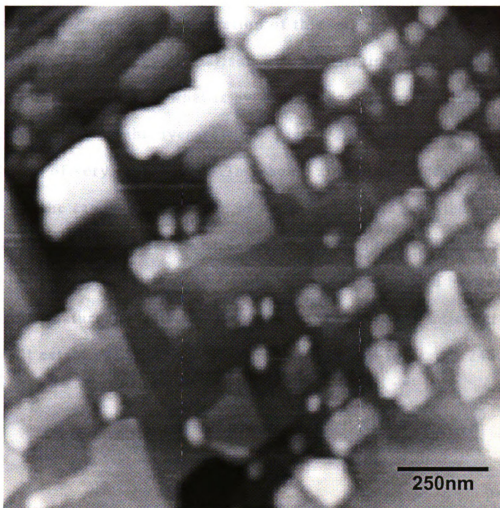


**Figure 22.** Unaltered, initial surface before exposure to sulfate, in non-doped, calcite equilibrated solution for 2 hours.

Figure 23 shows the surface after 4 hours in sulfate doped solution. Note that the location of this image is not the same as in Figure 22 so direct comparison with the original features is not possible. However, what is evident is the regular, unaltered morphology of the overgrowths. Figure 24a was captured after 17 hours of very slow flow (1.3mL/hour) aragonite saturated solution with the same concentration of sulfate. The exaggerated topography was difficult to image with large islands >150nm wide and >100nm high (the region shown in figure 24 is an area nestled between the large features). Detail of the terraces that filled in adjacent to the well established, polynuclear growth is shown in Figure 24b.

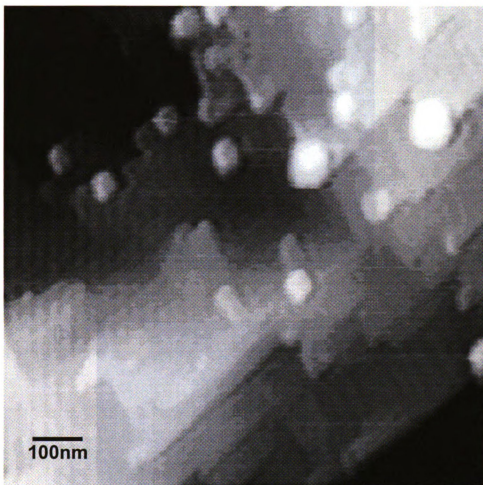


**Figure 23.** Surface after 4 hours in sulfate doped solution (10 μM SO<sub>4</sub>).

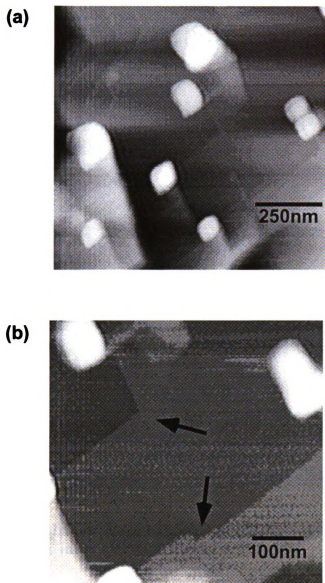


**Figure 24.** (a) Surface after 17 hours in slowly flowing  $\text{SO}_4$ -doped solution; (b) Detail of sulfate doped surface. Monolayer step height: 0.32nm. Note step morphology indicated by arrows.

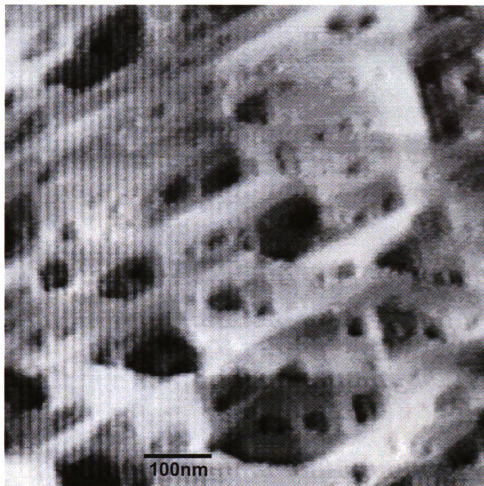


**Figure 25.** Initial Kola calcite surface immediately after first wetting in calcite equilibrated solution.

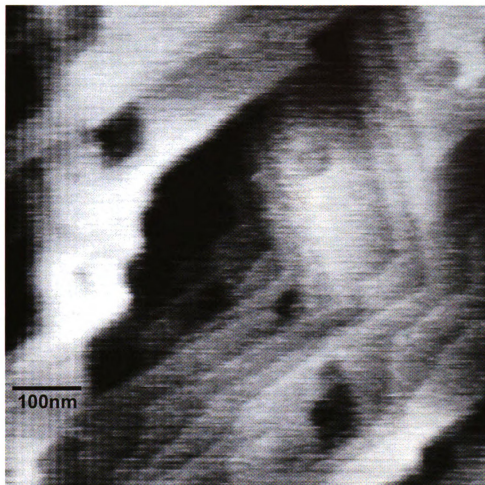


**Figure 26.** Filling in of surface features by new growth in non-doped solution.



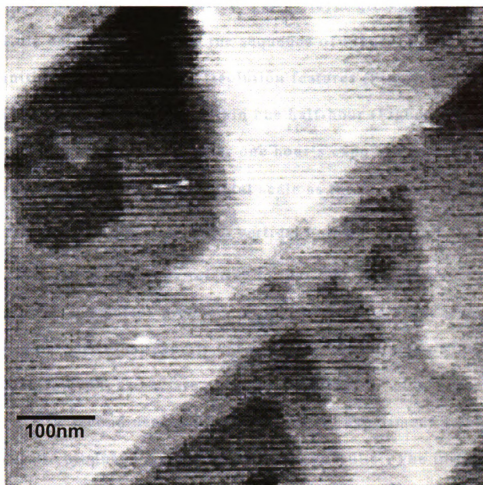


**Figure 27.** Surface after 1 hour in flowing sulfate-doped solution ( $10\mu\text{M SO}_4$ ).

Introduction of sulfate during layer growth on high-quality Kola calcite is shown in the sequence of Figures 25, 26, and 27. The initial “Swiss Cheese” dissolution features (Figure 25) began to fill-in at calcite saturation within one half-hour (Figure 26). Figure 27 shows the same region after one hour’s exposure to sulfate solution ( $10\mu\text{M}$ ) at the same horizontal scale as the previous images. While somewhat obscured by  $2\text{-}3\text{\AA}$  vertical noise, the monolayer steps retain a “clean” morphology relative to that seen in phosphate doped growth. The steps produced in  $\text{SO}_4$  bearing solution are not distorted in this individual experiment although, the corners of the central feature in Figure 27 are possibly distorted.

A second near-equilibrium, growth experiment using Kola calcite produced much less ambiguous results. The initial surface consisted of broad steps with none of the pitted structure of figure 25. Active growth was monitored by observing the tonguing island feature shown in Figure 28, imaged in non-doped solution after 1 hour. No nucleation was observed on the broad terraces ( $>100\text{nm}$ ) with classical step features. This feature was completely obscured by new growth as the experiment proceeded. Figure 29 (a and b) displays in broad view and detail, the regular step features of the terraces that overlaid the original tonguing-island feature after one hour of continuous flow of solution doped with  $10\mu\text{M}$   $\text{SO}_4$

(Electronic noise = 3 to 4Å, measured from a surface profile during force calibration).

The surface was then flushed with double the concentration of sulfate (20  $\mu$ M) at the same saturation. Under these conditions, steps retained very angular/regular morphology (Figure 30a). In order to ensure that scanning the same feature had not simply arrested all growth or otherwise altered the surface, the tip was moved to several different, previously un-scanned locations. At all sites imaged by relocating the AFM tip, the same step morphology was observed. Figure 30b shows the surface after an extended time (1.5 hours) at this higher sulfate concentration. Protruding features (i.e. tonguing on lower right of figure 30b) were eroded by scanning causing the apparent rounded corners.

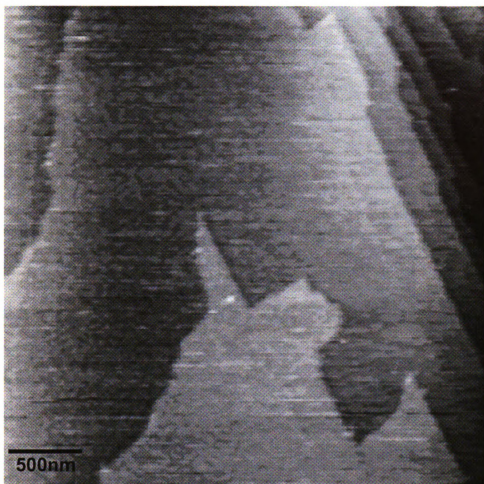
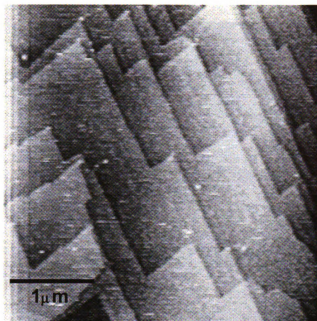


**Figure 28.** Tounging-island feature used to monitor growth progress. Initially imaged after 1 hour in non-doped solution.

(a)



(b)

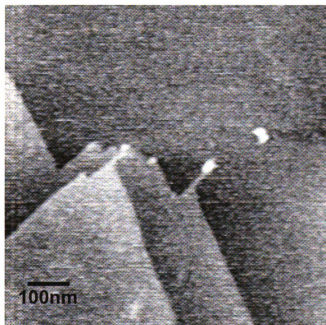


**Figure 29.** (a) Overgrowths after 1 hour in sulfate-doped solution; (b) Detail of steps imaged one minute later, and outside the region scanned in (a). Step height of pure calcite maintained at 0.38nm.

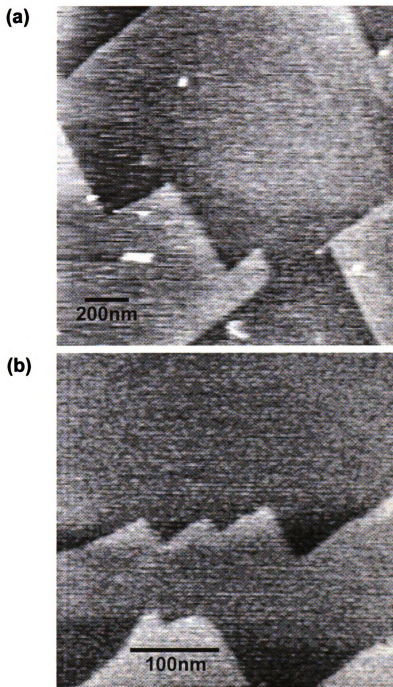


**Figure 30.** Overgrowths in the presence of  $20\mu\text{M SO}_4$ : (a) 30 minutes after surface flush with higher concentration solution; (b) detail of steps in adjacent region 1.5 hours later.

## **Phosphate Doped Growth**

The addition of phosphate to growth solutions significantly altered the surface morphology of both early nucleation and lateral step growth. These findings are in good agreement with previous AFM experiments performed by Dove and Hochella (1993). Here, early nucleation and layer growth was observed in both calcite and aragonite saturated solutions with  $\text{PO}_4$  concentrations ranging from 6 to 23  $\mu\text{M}$ .

In an experiment sequence similar to that exhibited in Figures 25-27, a very rough crystal surface covered with dissolution features was initially engaged in non-doped calcite saturated solution, (Figure 31). Growth continued in flowing, near equilibrium solution for 2 hours with growth occurring primarily at topographic high spots and step apices, while straight steps appeared immobile (Figure 31b).

Introduction of phosphate doped (12  $\mu\text{M}$ ), near equilibrium solution resulted in rounding of rhombohedral islands within five minutes of flushing with the solution (Figure 32). Continued flow of doped solution increased the distortion of overgrowth features. After 3 hours, islands of 30 to 400 nm across were all amorphous regardless of location on the crystal (Figure 33a and b). In a separate experiment with a solution equilibrated with calcite at a high  $\text{P}_{\text{CO}_2}$ , then allowed to degas, and a phosphate concentration of 23  $\mu\text{M}$ , nucleation was abundant and amorphous (Figure 34).

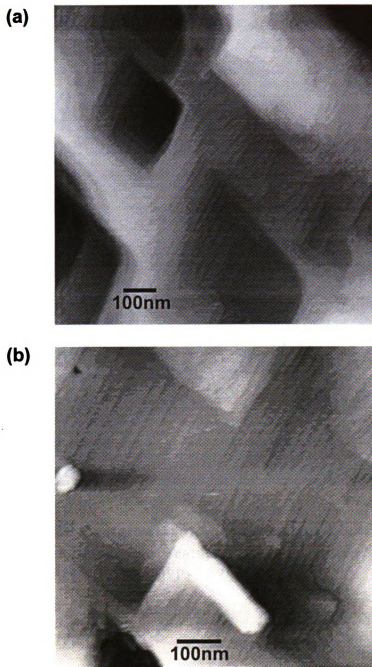


**Figure 31.** Initial surface used for phosphate experiment:  
(a) within 5 minutes of first wetting in non-doped solution;  
(b) same crystal and solution after 2 hours of continuous flow.



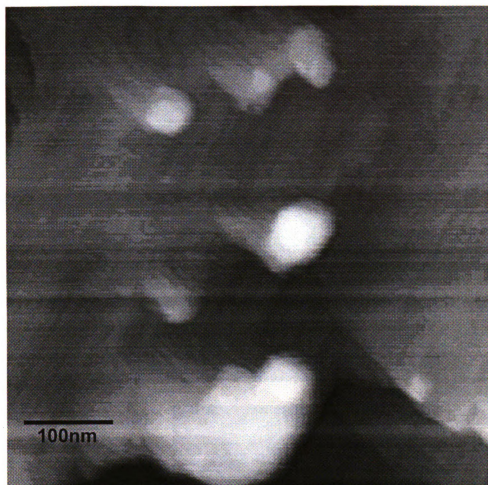


**Figure 32.** Overgrowths in the presence of  $12\mu\text{M PO}_4$ : immediate rounding of features occurred within 5 minutes of first exposure to  $\text{PO}_4$ -doped solution.

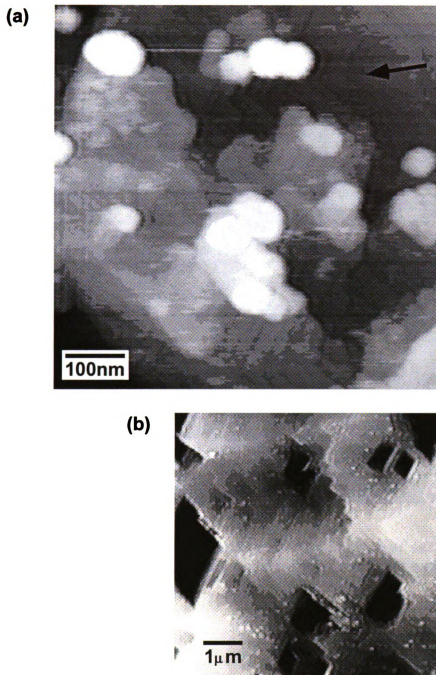


**Figure 33.** Growth features after 3 hours in  $\text{PO}_4$ -doped solution: (a) note unaltered topography of the substrate indicated by the arrow; (b) at lower magnification gross-scale morphology appears unaltered.

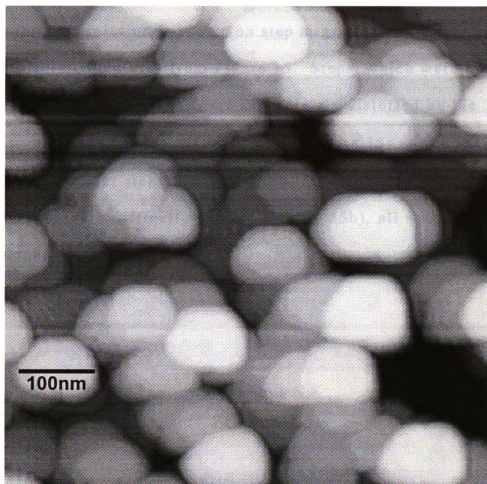


**Figure 34.** Amorphous islands covering surface of surface in flowing  $\text{PO}_4$ -doped ( $23\mu\text{M}$ ), calcite supersaturated solution for 2 hours.

The effect of phosphate on lateral step growth in aragonite saturated solution is shown on step migration across the same malformed features from Figure 15. Steps, which were very straight in non-doped solution, were immediately distorted by the introduction of phosphate (12  $\mu\text{M}$ ). Figure 35a shows the initial, very irregular steps that continued to degrade, until the surface became very difficult to image (Figure 35b), all within 2 minutes of doped solution flush.

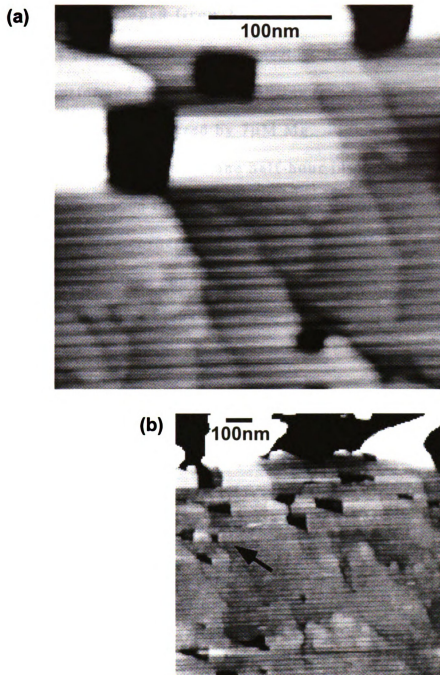


**Figure 35.** Distortion of mobile steps due to  $\text{PO}_4$  poisoning ( $12\mu\text{M}$ ): (a) immediately after introduction of doped solution; (b) continued degradation of the surface within 2 minutes. Arrow indicates approximate scanning area of (a).

## **Magnesium Doped Growth**

A limited number of magnesium doped growth experiments were performed. At near equilibrium conditions growth morphology was not radically altered by 7 $\mu$ M Mg. Figure 36 shows the detail of a monolayer corner after one half-hour in doped solution. The same results were seen in a later, identical experiment. At larger scales (2-5  $\mu$ m), step corners appeared to be smoothly rounded unlike any seen in non-doped conditions (Figure 37a). On closer inspection however, angular kinks along the step edge are apparent (Figure 37b).

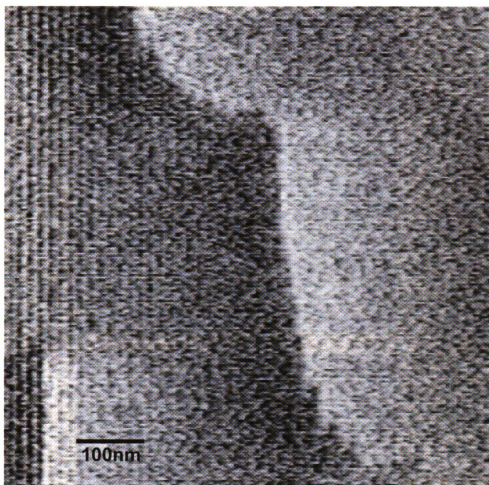


**Figure 36.** Mg-doped surface, somewhat obscured by scanner noise.

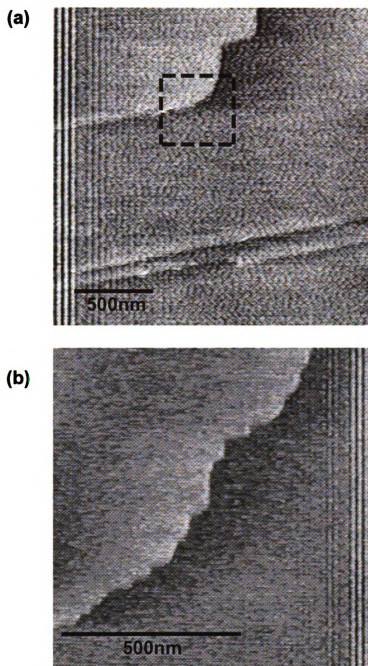


**Figure 37.** (a) Monolayer growth in Mg-doped ( $7\mu\text{M}$ ) solution. (b) Detail of rounded step corner.



## CONCLUSIONS

### **Nano-Morphology of Calcite in Complex Solutions**

Magnesium, phosphate and sulfate are just a few of the important major ions in seawater and have been demonstrated to be strong calcite precipitation inhibitors. The effects of two of these ions on calcite precipitation have already been demonstrated through nano-scale AFM analysis.

In the experiments performed for this research,  $\text{PO}_4^{3-}$  ions produced rounded, amorphous nuclei when introduced in early growth stages (similar to Dove and Hochella, 1993). These observations were verified to be actual amorphous features rather than simply a poor image, a bad tip or other artifact, by re-growing non-doped nuclei on the same crystal. When orthophosphate doped solutions (6 to 23  $\mu\text{M}$ ) were introduced to surfaces undergoing lateral step growth, step edges were quickly altered to become ragged and irregular. The results from these phosphate experiments show good agreement with previous workers. In a small number of experiments, magnesium (7 $\mu\text{M}$ ) had a slight effect on the morphology of step corners, also in agreement with previous studies.

Evidence presented in this study suggests that the  $\text{SO}_4^{2-}$  anion is incorporated into the calcite lattice at  $\text{CO}_3^{2-}$  sites. During early growth stages (nucleation), no effect was observed in the presence of

$\text{SO}_4^{2-}$ . Crystallites and islands retained the regular rhombohedral habit of non-doped calcite. When introduced to crystals undergoing active layer growth,  $\text{SO}_4^{2-}$  did little to alter the morphology of step edges. It is concluded that the mechanism of sulfate growth inhibition at the calcite surface, within the range of sulfate concentrations used for these experiments (10 to 20  $\mu\text{M}$ ), includes the incorporation of the sulfate anion into the crystal lattice.

Given the complexity of natural waters, there are still many effects that remain to be observed and quantified. Composite effects of multiple inhibitors (and catalysts) and the resulting crystal growth processes have many diagenetic implications (Matty and Tomson, 1988). AFM technology, used in concert with other surface analytical techniques, will continue to be an invaluable tool in the study of complex surface textures and reactions.

### **Atomic Force Microscopy**

Atomic Force Microscopy is a young technology and it is proving to be a powerful tool with numerous applications. In the study of mineral-water interactions, AFM observations are helping to confirm and refine existing geochemical and crystal growth models. The non-destructive, in-situ and near atomic scale capabilities of the AFM allows for the observation of reacting surfaces at high resolutions.

The ability to nondestructively image microtopographic features of mineral surfaces may outweigh the limitations of the method, provided these limitations are accounted for within the interpretation of the results. Combined with a suite of analytical methods the whole picture can be developed. In-situ x-ray methods are being employed to observe the structure of the mineral-water interface (Chiarello and Sturchio, 1994; Chiarello et al, 1993), and these recent advancements in microscopic technologies have opened the door for better understanding of the solid-solution interface. Mutual verification between technologies makes each a much more powerful tool.

## **APPENDIX**

## **APPENDIX**

### **FORCE CALIBRATION**

The force exerted on the surface by the tip is determined in a calibration routine by holding the cantilever stationary in the horizontal (x, y) direction while moving the cantilever a known distance along the vertical (z) axis. Electronically adjusting the window of movement in the z direction, relative to an electronic setpoint, increases or decreases the force on the sample.

The force experienced by the surface is calculated by  $F=k\Delta Z$ . Where  $k$  is the spring constant determined by the tip manufacturer (Digital Instruments, 1995) and  $\Delta Z$  is the separation between the setpoint control point and the point at which the tip pulls off of the surface (Figure A1). Average separation measured during the course of these experiments was  $\approx 70\text{nm}$  producing an average force of 2 to 20nN, depending on the tip spring constant used.

## APPENDIX

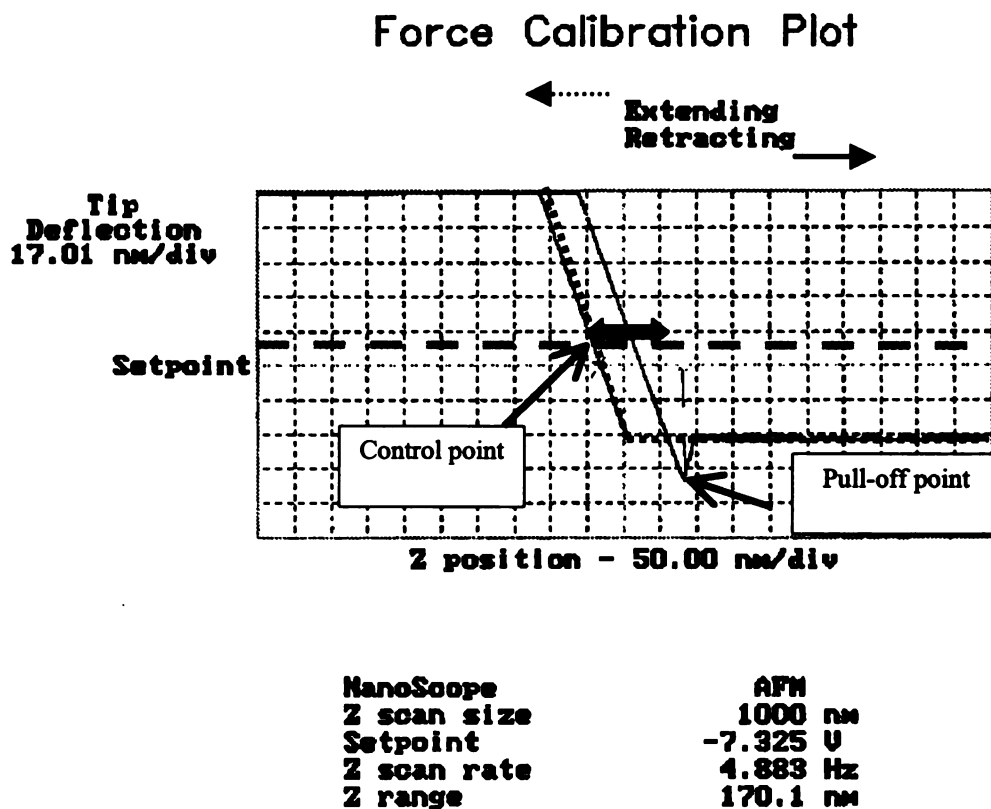


**Figure A1.** Example of Force calibration Plot generated during these experiments.  $\Delta Z$  is indicated by the double-headed arrow.

## **LIST OF REFERENCES**

## LIST OF REFERENCES

- Berner, R. A., (1975). "The role of Magnesium in the Crystal Growth of Calcite and Aragonite from Sea Water." *Geochimica et Cosmochimica Acta*, 39, pp. 489-504.
- Berner, R., and Morse, J., (1974). "Dissolution kinetics of calcium carbonate in seawater: Theory of calcite dissolution." *American Journal of Science*, 274, pp. 108-134.
- Binning, G., Quate, C. F. and Gerber, C., (1986). "Atomic Force Microscope." *Physical Review Letters*, 56, pp. 930-933.
- Bischoff, J. L., and Fyfe, W. S., (1968). "Catalysis, Inhibition, and the Calcite-Aragonite Problem." *American Journal of Science*, 266, pp. 65-79.
- Bosbach, D., Junta-Rosso, J. L., Becker, U. and Hochella, M. F., (1996). "Gypsum growth in the presence of background electrolytes studied by Scanning Force Microscopy." *Geochimica et Cosmochimica Acta*, v. 60, No. 17, pp. 3295-3304.
- Burton, W. K., Cabrera, N., and Frank, F. C., (1951). "The growth of crystals and the equilibrium structure of their surfaces". *Royal Soc. of London Phil. Trans.*, A-243, p. 299-358.
- Burton, E., and Walter, L., (1987). "Relative precipitation rates or aragonite and Mg calcite from seawater: Temperature or carbonate ion control?" *Geology*, 15, p. 111-114.
- Brewer, P. G., (1975). *Chemical Oceanography*. V. 1., J. P. Riley and G. Skirrow Eds., Academic, New York, 223pp.
- Burton, E., and Walter, L., (1990). "The role of pH in phosphate inhibition of calcite and aragonite precipitation rates in seawater." *Geochimica et Cosmochimica Acta*, 54, pp. 797-808.
- Busenberg, E., and Plummer, N. (1985) "Kinetic and thermodynamic factors controlling the distribution of  $\text{SO}_4^{2-}$  and  $\text{Na}^+$  in calcites and selected aragonites." *Geochimica et Cosmochimica Acta*, 49, pp. 713-725.
- Cheng L., Lyman P., Sturchio N. C. and Bedzyk M. J., (1997). "Adsorption and structure of selenite anions on the calcite (1014) surface." *Surface Science* 382, L690-L695.



- Chiarello, R. P. and Sturchio, N. C., (1994). "Epitaxial growth of otavite on calcite observed in situ by synchrotron X-ray scattering." *Geochimica et Cosmochimica*, 58, pp. 5633-5638.
- Chiarello, R. P. and Sturchio, N. C., (1995). "The calcite (1014) cleavage surface in water: Early results of a crystal truncation rod study." *Geochimica et Cosmochimica*, 59, pp. 4557-4561.
- Cowan, C. E., Zachara, J. M. and Resch, C.T (1990). "Solution effects on the surface exchange of selenite on calcite." *Geochimica et Cosmochimica Acta*, 54, pp. 2223-2234.
- Deleuze, M. and Brantley, S. L., (1997). "Inhibition of calcite crystal growth by  $Mg^{2+}$  at 100°C and 100bars: Influence of growth regime." *Geochimica et Cosmochimica Acta*, 61, pp. 1475-1485.
- Didymus, J., Oliver, P., Mann, S., DeVries, A., Hauschka, P. and Westbroek, P., (1993). "Influence of low-molecular and macromolecular organic additives on the morphology of calcium carbonate." *J. Chem. Soc. Faraday Trans.*, 89, pp. 2891-2900.
- Digital Instruments (1995). *NanoScope Reference Manual, Update Version 4.10*. Digital Instruments, Santa Barbara California, USA. [www.di.com](http://www.di.com)
- Dove, P., and Chermak, J. (1994). "Mineral-water interactions: Fluid cell applications of Scanning Force Microscopy." In *Scanning Probe Microscopy of Clay Minerals*, Nagy and Blum eds., The Clay Minerals Society, CMS Workshop Lectures, Vol. 7, pp. 140-169.
- Dove, P., Hochella, M., and Reeder, R. J., (1992). "In situ investigation of near-equilibrium calcite precipitation by atomic force microscopy." In *Rock Water Interactions, Low Temperature Environments*, Kharaka, Y.K. and Maest, A.S, eds., *Proceedings of 7th International Symposium on Water-Rock Interaction*, Park City Utah, pp. 141-144.
- Dove, P., and Hochella, M. (1993) "Calcite precipitation mechanisms and inhibition by orthophosphate: In situ observations by Scanning Force Microscopy" *Geochimica et Cosmochimica Acta*, 57, pp. 705-714.
- Drake, B.; Hellmann, R.; Sikes, C. S. and Occelli, M. L., (1992). "Atomic scale imaging of albite feldspar, calcium carbonate, rectorite and bentonite using Atomic Force Microscopy." *SPIE Vol. 1639 Scanning Probe Microscopies*, pp. 151-159.

- Eggleston, C. M., (1994). "High Resolution Scanning Probe Microscopy: Tip-surface interaction, artifacts and applications in mineralogy and geochemistry" in Scanning Probe Microscopy of Clay Minerals, Nagy and Blum ed. The Clay Minerals Society, CMS Workshop Lectures, Vol. 7, pp.
- Gratz, A. J., Hillner, P., Manne, S., and Hansma, P. K., (1992). "Dynamic Studies of Crystal growth Using the AFM." In Scanning Probe Microscopies, S. Manne ed., SPIE, 1639, pp. 182-185.
- Gratz, A. J., Hillner, P., and Hansma, P. K., (1993). "Step dynamics and spiral growth on calcite" *Geochimica et Cosmochimica Acta*, 57, pp. 491-495.
- Gratz, A. J. and Hillner, P., (1993). "Poisoning of calcite growth viewed in the atomic force microscope (AFM)." *Journal of Crystal Growth*, 129, pp.789-793.
- He, S. and Morse, J. W., (1993). "The carbonate acid system and calcite solubility in aqueous Na-K-Ca-Mg-Cl-SO<sub>4</sub> solutions from 0 to 90°C. *Geochimica et Cosmochimica Acta*, 57, pp. 3533-3554.
- Hillner, P., Gratz, A. J., and Hansma, P. K., (1992). "Atomic-scale imaging of calcite growth and dissolution in real time." *Geology*, 20, pp. 359-362.
- Hillner, P. E., Manne, S., Hansma, P. K., and Gratz, A.J., (1993). "Atomic Force Microscope: A New Tool for Imaging Crystal Growth Processes." *Faraday Discussions*, 95, pp. 191-197.
- Hochella, M.F., (1990). "Atomic structure, microtopography, composition and reactivity of mineral surfaces." In *Mineral-Water Interface Geochemistry*, Hochella, M.F and White, A. F., eds., Mineralogical Society of America Reviews in Mineralogy, 23, pp. 87-132.
- House, W.A. and Donaldson, L., (1986). "Adsorption and coprecipitation of phosphate on calcite." *Journal of Colloid and Interface Science*, 112, pp. 309-324.
- Kipp, S., Lachmann, R., and Schneeweiss, M.A., (1994). "Methods and apparatus for in situ investigation with the scanning force microscope." *Journal of Crystal Growth*, 141, pp. 291-298.
- Klein, C. and Hurlbut, C.S.Jr., (1985). *Manual of Mineralogy*, 21<sup>st</sup> edition. John Wiley & Sons, New York. 681p.
- Liang, Y.; Lea, A. S.; Baer, D. R.; and Engelhard, M. H. (1996). "Structure of the Cleaved CaCO<sub>3</sub>(101bar4) Surface in an Aqueous Environment." *Surface Science*, v. 351, 1-3, pp. 172-182.

- Livingstone, A. D., (1963). Chemical Components of Rivers and Lakes. USGS paper No. 440G.
- Matty, J. M. and Tomson, M. B., (1988). "Effect of multiple precipitation inhibitors on calcium carbonate nucleation." *Applied Geochemistry*, 3, pp. 549-556.
- Morse, J. W., (1983;1990). "The kinetics of calcium carbonate dissolution and precipitation." In *Carbonates: Mineralogy and Chemistry*, Reeder, R.J. Ed. *Reviews in Mineralogy*, 11, pp. 227-264.
- Mucci, A., Canuel, R., and Zhong, S. (1989) "The solubility of calcite and aragonite in sulfate-free seawater and the seeded growth kinetics and composition of the precipitates at 25C." *Chemical Geology*, 74, pp. 309-320.
- Mucci, A., and Morse, J. (1984). "The solubility of calcite in seawater solutions of various magnesium concentration,  $I=0.697m$  at 25C and one atmosphere total pressure." *Geochimica et Cosmochimica Acta*, 48, pp. 815-822.
- Mucci, A., and Morse, J. (1985). "Auger spectroscopy determination of the surface-most adsorbed layer composition of aragonite, calcite, dolomite, and magnesite in synthetic seawater." *American Journal of Science*, 285, pp. 306-317.
- O'hara, M. and Reid, R.C., (1973). *Modeling Crystal Growth Rates from Solution*, 272p.
- Paquette, J., Hojatollah, V. and Mucci, A., (1996). "TEM study of Pt-C replicas of calcite overgrowths precipitated from electrolyte solutions." *Geochimica et Cosmochimica Acta*, 60, pp. 4689-4699.
- Paquette, J. and Reeder, R.J., (1990). "New type of compositional zoning in calcite: Insights into crystal-growth mechanisms." *Geology*, 18, pp. 1244-1247.
- Paquette, J. and Reeder, R.J., (1995). "Relationship between surface structure, growth mechanism, and trace element incorporation in calcite." *Geochimica et Cosmochimica Acta*, 59, pp. 735-749.
- Prater, C. B, Maivald, P. G; Kjoller, K. J.; and Heaton, M. G.; (1995). "Probing Nano-scale Forces with the Atomic Force Microscope." *Monograph, Digital Instruments, Santa Barbara California*. 16pp.
- Rasband, W. (1997). NIH Image 1.60. National Institutes of Health, USA. <http://128.23.16/nih-image>

Reddy, M. M., (1986). "Effect of magnesium ions on calcium carbonate nucleation and crystal growth in dilute aqueous solutions at 25°C." In *Studies in Diagenesis*, Mumpton, F.A. Ed., U.S. Geological Survey Bulletin, pp. 169-182.

Reeder, R. J., Lamble, G. M., Lee, J., and Staudt, W. J., (1994) "Mechanism of  $\text{SeO}_4^{2-}$  substitution in calcite: An XAFS study." *Geochimica et Cosmochimica Acta*, 58, pp. 5639-5646.

Staudt, W.J., Reeder, R.J., and Schoonen, M.A.A., (1994) "Surface structural controls on compositional zoning of  $\text{SO}_4^{2-}$  and  $\text{SeO}_4^{2-}$  in synthetic calcite single crystals." *Geochimica et Cosmochimica Acta*, 58, pp. 2087-2098.

Stipp, S., Eggelston, C.M., and Nielsen, B., (1994) "Calcite surface structure observed at microtopographic and molecular scales with atomic force microscopy (AFM)" *Geochimica et Cosmochimica Acta*, 58, pp. 3023-3033.

Stumm, W., (1992). *Chemistry of the Solid-Water Interface*. John Wiley & Sons, New York. 428p.

Sunagawa, I., (1984). "Growth of Crystals in Nature", in *Materials Science of the Earth's Interior*, Sunagawa, I., ed. *Materials Science of Minerals and Rocks*, Terra Scientific. pp. 63-105.

Takano, B., (1985). "Geochemical implications of sulfate in sedimentary carbonates." *Chemical Geology*, 49, pp. 393-403.

Walter, L. (1986). "Relative efficiency of carbonate dissolution and precipitation during diagenesis: A progress report on the role of solution chemistry" in *Roles of Organic Matter in Sediment Diagenesis*, Gautier ed. U.S.G.S. Society of Economic Paleontologists and Mineralogists Special Publication No. 38. pp. 1-11.

Walter, L. and Morse, J. (1984). "Magnesian calcite stabilities: A reevaluation." *Geochimica et Cosmochimica Acta*, 48, pp. 1059-1069.

Walter, L. and Morse, J. (1985). "The dissolution kinetics of shallow marine carbonates in seawater: A laboratory study." *Geochimica et Cosmochimica Acta*, 49, pp. 1503-1513.

Wiesendanger, R., (1994). *Scanning Probe Microscopy and Spectroscopy, Methods and Applications*. Cambridge University Press, 637p.

MICHIGAN STATE UNIV. LIBRARIES



31293017128905